ANL K75 -3191 - 1

PRELIMINARY EVALUATION

OF TWO-ELEMENT OPTICAL CONCENTRATORS

FOR USE IN

SOLAR PHOTOVOLTAIC SYSTEMS

SPECTROLAB, INC.

JUNE 30, 1975

PREPARED FOR

U of C-AUA-USERDA

ARGONNE NATIONAL LABORATORY, ARGONNE, ILLINOIS

operated under contract W-31-109-Eng-38 for the

U. S. ENERGY RESEARCH AND DEVELOPMENT ADMINISTRATION

DISCLAIMER

ANL - K75 - 3191 - 1

Distribution Category:
Solar Thermal (UC-62)

PRELIMINARY EVALUATION

OF TWO-ELEMENT OPTICAL CONCENTRATORS

FOR USE IN

SOLAR PHOTOVOLTAIC SYSTEMS

SUBMITTED TO

ARGONNE NATIONAL LABORATORY

SUBCONTRACT 31-109-38-3191

SPECTROLAB, INC.

30 JUNE 1975

INTRODUCTION

This report presents the results of the work performed by Spectrolab, Incorporated, supported by D. L. Evans, L. W. Florschuetz and B. D. Wood of Arizona State University as consultants, for Argonne National Laboratory under Letter Subcontract 31-109-38-3191.

The Statement of Work for this program was:

Objective: To evaluate for photovoltaic applications the use of the CPC design as a field collector - in conjunction with a primary focusing concentrator. The primary focusing concentrator may be a parabolic reflector, an array of Fresnel mirrors, a Fresnel lens or some other type.

1. Select several candidate configurations of such compound systems (focusing concentrators/CPC field collectors).
2. Perform an analytic evaluation of the technical performance of these systems.

   This evaluation should include consideration of:

   a) Optimal concentration ratio.

   b) Distribution of energy flux across the cell surface and how this relates to cell design and performance when used with CPC concentrator.

   c) Operating temperature of cell and method for rejecting heat; techniques for passive ambient air cooling and active fluid cooling should be considered and evaluated.

3. Identify the most promising configurations and perform a cost effectiveness study pertinent to coupling CPC concentrators to solar cells.
4. Prepare a report on the work performed under the above tasks, detailing the results and conclusions obtained, and deliver ten copies of the final report to the Argonne National Laboratory prior to 30 June, 1975.

This report consists of six chapters, of which this introduction is the first. The second chapter derives design equations for the CPC secondary element in an optimum two-element concentrating system, and discusses the performance of this two-element system and the choice of the primary element. The third chapter, written by D. L. Evans of ASU, presents the results of ray-tracing calculations to investigate the uniformity of illumination at the absorber. The fourth chapter, written by L. W. Florschuetz of ASU, discusses the heat transfer problem, especially the use of the CPC element as an extended surface for heat rejection to ambient air. The fifth chapter briefly relates the preceding results to the cost-effectiveness calculations previously performed by us under NSF sponsorship. The final chapter summarizes our results and conclusions. The program manager for this program and the author of this report (except for the third and fourth chapters) is F.T.C. Bartels of Spectrolab.

Most of the work reported here was done during a period of four weeks, and the short time available for the program resulted in a less well integrated report than we would have liked to present. For example, the ray-tracing calculations in Chapter 3 assumed the CPC surfaces were parabolas; actually they are ellipses, as derived in Chapter 2, but the

results of Chapter 2 were not available to Don Evans early enough. The difference is not important to the conclusions drawn, though. We also decided not to perform any new cost-effectiveness calculations for this report because we felt that we would not be able to improve on the material already presented in our NSF report without detailed consideration of specific system designs and applications, and there was no time for that.

Optical concentrators have been extensively investigated in connection with systems which collect solar energy for utilization in the form of thermal energy. If photovoltaic cells are used as the absorber, direct conversion of part of the incident solar energy to electricity can be achieved in a very simple way, and the remainder of the incident energy is converted to heat and may be utilized in that form. However, the efficiency of photovoltaic conversion decreases with increasing cell temperature, and also, in general, with increasing illumination intensity due to cell and interconnect series resistance.

Taking these factors into account results in a set of requirements for an optical concentrator for use with photovoltaic cells, which differs considerably from the requirements of a solar-thermal system. In particular, it is very important to secure uniform illumination of the absorber, since cell resistance losses are proportional to the local, rather than the average, illumination intensity. Previous work with single-element concentrators showed that very large ratios of peak local to average intensity could be expected; the ray tracing of the parabolic trough (Chapter 3)

yields a value of about 15 for this ratio, which is typical of calculated values for several types of single-element concentrators. Measured values are lower because of deviations from perfect figure, but are still high enough to be very troublesome to the designer. The CPC or "Winston" concentrator is much better in this regard; the ray tracing in Chapter 3 yields a ratio of about 3. However, the CPC is quite uneconomic at concentration ratios of 10 to 50 which are the most cost-effective.

The ray tracing calculations show that the two-element system consisting of a parabolic trough and a CEC (compound elliptical concentrator) provides a local/average ratio of 1.2 for on-axis illumination. Off-axis ray tracing was not completed in time for this report; the ratio is slightly worse, but not so much as to present a problem. The demonstration that excellent uniformity of absorber illumination can be obtained in a low-cost concentrator is the most important result of this program.

In all other respects investigated, the two-element concentrator is also an attractive choice. We therefore have no reservations in recommending that more effort be expended on this design concept.

The authors of this report gratefully acknowledge the contributions of Dr. Roland Winston to the work presented here. Dr. Winston generously made available to us his latest work in advance of publication, and also other ANL work which we did not know existed. The importance of his contributions is evident throughout this report.

CONCENTRATOR DESIGN EQUATIONS

We desire to determine the design parameters and performance of an optical system for solar energy concentration consisting of a parabolic trough and a secondary concentrator of the "Winston" type. A cross section of the system to be analyzed is shown in Figure 1, which also defines the symbols used.

Direct solar radiation is incident upon the primary mirror P from the right, and is considered to be contained within an angular field of view $\pm \delta$. Rays incident upon the primary mirror at its edges F, F' are deviated through an angle θ. The aperture $\overline{CC'}$ of the secondary element is placed at the focal point of the primary, and $\overline{CC'}$ is taken just large enough so that all direct solar radiation incident upon the primary mirror enters the aperture.

We desire to determine the surfaces S, S' subject to the conditions that all of the direct solar radiation entering the aperture $\overline{CC'}$ will strike the absorber $\overline{F'F}$, and that isotropic diffuse radiation reflected from the primary mirror will also be concentrated by the secondary element to the maximum extent possible. Winston (1) has shown that maximum concentration of diffuse radiation from a source of limited length at a finite distance from the concentrator aperture is achieved if S and S' are segments of ellipses with foci at F, F and F', F' respectively.

We can therefore write:

$q = \overline{FC} = \overline{F'C'} = (m+1) \csc(\theta + \delta)$

$p = \overline{FC'} = \overline{F'C} = (m-1) \csc(\theta - \delta)$

$r = \overline{CF} = \overline{C'F'}$

$q + r = p + r + 2Z^{-1}$

$2Z^{-1} = (q - p)$

which confirms the conservation of phase space in the secondary concentrator, as shown by Winston. Note that the half-aperture of the secondary concentrator is taken as unity, so that Z is the concentration factor of the secondary element and (m -1) is the concentration factor of the primary element, allowing for the shadowing effect of the secondary.

After a little manipulation, we find:

$m = \sin 2\theta \csc 2\delta$

$Z = \cos \delta \csc \theta$

The total concentration factor is

$M = Z(m-1)$

The length of the secondary element is

$y = (Z+1) / Z \tan(\theta - \delta)$

and the spacing between the aperture planes is

$f = m \operatorname{ctn} \theta$

The value of θ for which M is a maximum, for a given δ, can be found from the relationship

$$2 \sin^3 \theta = \sin 2\delta \cos \theta$$

and substituting the value of θ thus found into the preceding equations defines the geometry of the optimum concentration system.

Table I gives the calculated values of the optimum design parameters for values of δ between 0.25° and 10°. These values are also plotted in Figure 2. Table I also gives, for comparison purposes, the concentration factor M_w and length y_w of a single-element CPC and the concentration factor M_p of an optimized parabolic trough alone ($\theta = 45°$), calculated for the same values of δ and effective primary aperture $2(m-1)$ as for the two-element system. For the largest values of δ listed in Table I, the two-element concentrator design is probably more costly than a truncated CPC. However, for concentration ratios above 10, the two-element design provides almost as much concentration as the ideal concentrator, while requiring much less reflective surface. In fact, for small values of δ the two-element concentrator requires less reflective surface than an optimum parabolic trough of equal aperture, while providing nearly twice the concentration.

Little change in overall performance results if an off-optimum choice of design parameters is made. Table II gives calculated parameters of two sets of designs. The first section of Table II shows the results of varying θ from 5° to 45°, choosing the remaining parameters for a value of $\delta = 1°$. The second section shows the result of fixing $\theta = 30°$, which essentially fixes the design of the secondary element for small δ. For $\delta = 1°$, the off-optimum design with $\theta = 30°$ yields a concentration ratio 83% of the ideal, while the optimum two-element design with $\theta = 14.86°$

attains 90% of the ideal.

Table II thus shows that the entire range of interest of δ and M can be covered quite well with a single secondary concentrator element, scaling the primary mirror for different values of δ and M. This is an important practical consideration for a number of reasons. The most important is that the secondary element, because of its small size, can be fabricated as an aluminum extrusion, thus providing the required structural support and heat transfer surface for the photovoltaic cells as well as the additional optical concentration at very low manufacturing cost. This cost advantage would not be obtained if it were necessary to design and tool for a large number of secondary elements in order to cover all applications.

Finally, we note that the primary element is specified only by the parameters m and θ. Although we have not made detailed calculations, it is apparent that primary elements other than a parabolic trough could be used with a similar improvement in performance. The choice of primary element should be made on the basis of cost per unit aperture area, and on the required characteristics specific to a given application. Since the available time does not permit us to develop designs and cost data for specific applications, we can only suggest some possibilities for future consideration.

Tabor and Zeimer (2) have considered the circular trough, and Baum and Strong (3) have compared the performance of a two-element system consisting of a spherical primary and an ellipsoidal secondary to a single-element paraboloid. These results suggest that the aberrations

associated with a circular or spherical primary can actually be used to advantage in a two-element system. In addition, a circular primary is probably less expensive to manufacture.

Tabor (4) has also considered using the primary parabola off-axis to eliminate shadowing. For $\delta = 7.5°$, Tabor calculated that an optimized parabolic trough with the absorber located off-axis would attain a concentration ratio of 3.24, compared to 2.86 with the absorber on-axis. By adding a plane mirror as a secondary concentrator, the attainable concentration factor was increased to 3.69. If a CEC concentrator is used as a secondary element in the on-axis configuration, the maximum concentration factor is 4.7 (from Figure 2) using a CEC with a concentration factor of 2.05. In the off-axis configuration with the same CEC concentrator an overall concentration factor of 6.1 is attainable, using Tabor's equations for the off-axis parabola. This suggests that two-element systems with off-axis mounting of the secondary may be attractive for the large values of δ associated with non-tracking seasonally-adjusted concentrators.

The fixed mirror solar concentratorproposed by John L. Russell, Jr. of General Atomic Company might also benefit from the addition of a CEC as a secondary element. The Russell concentrator (5) uses a fixed Fresnel-type mirror and a moveable collector to attain concentration ratios as high as 40 to 50. However, such a high ratio requires a large number of mirror facets with highly accurate alignment, which conflicts with the intended objective of making the primary mirror very inexpensive.

The addition of a CEC should relax the primary mirror specifications and lead to cost savings.

In some applications lenses may be preferred to mirrors. Fresnel lens can be made quite cheaply from glass or plastic by molding processes, with acceptable accuracy for solar concentration purposes. For a single lens, ideal performance would require a relative aperture of $f/0.5$ which is the theoretical limit for a lens. Single-lens concentrators are probably impractical beyond $f/1.0$ because of large losses from internal reflection. The addition of a CEC secondary element should permit near-ideal performance to be obtained from a lens of practical relative aperture. Also, linear Fresnel lenses exhibit a defocusing problem (6) not exhibited by reflective linear concentrators; this is illustrated in Figures 3, 4 and 5. Meridional rays not normal to the lens plane are focused at a point closer to the lens than normal rays, leading to a loss of energy from the outer edges of the lens as the sun moves away from the lens normal. It would appear that the addition of a CEC secondary element would eliminate the effects of this behavior.

Thus we feel that, in addition to the parabolic trough in the on-axis configuration analyzed in detail above, other choices of the primary element which might be best in a particular situation are the circular trough, fixed Fresnel mirror and Fresnel lens. Both the circular and parabolic troughs might also be used in an off-axis configuration. The three-dimensional analogs of these two-dimensional elements culd also be added to the list. Practical designs for each of these primary elements fall far short of ideal performance and therefore their performance can

be significantly improved by addition of a low-power CEC.

References:

(1) R. Winston: Ideal Light Collectors in Cylindrical Geometry; ANL note 4/13/75.

(2) H. Tabor and H. Zeimer: Low-Cost Focussing Collector for Solar Power Units; Solar Energy 6, 55-59 (1962).

(3) W. A. Baum and J. D. Strong: Basic Optical Considerations in the Choice of a Design for a Solar Furnace; Solar Energy 2, No. 3-4, pp. 37-45 (1958).

(4) H. Tabor: Stationary Mirror Systems for Solar Collectors; Solar Energy 2, No. 3-4, pp. 27-33 (1958).

(5) J. L. Russell, Jr. et al: Principles of the Fixed Mirror Solar Concentrator; General Atomic Co. Report GA-A12902 (1974).

(6) D. L. Evans: Private communication.

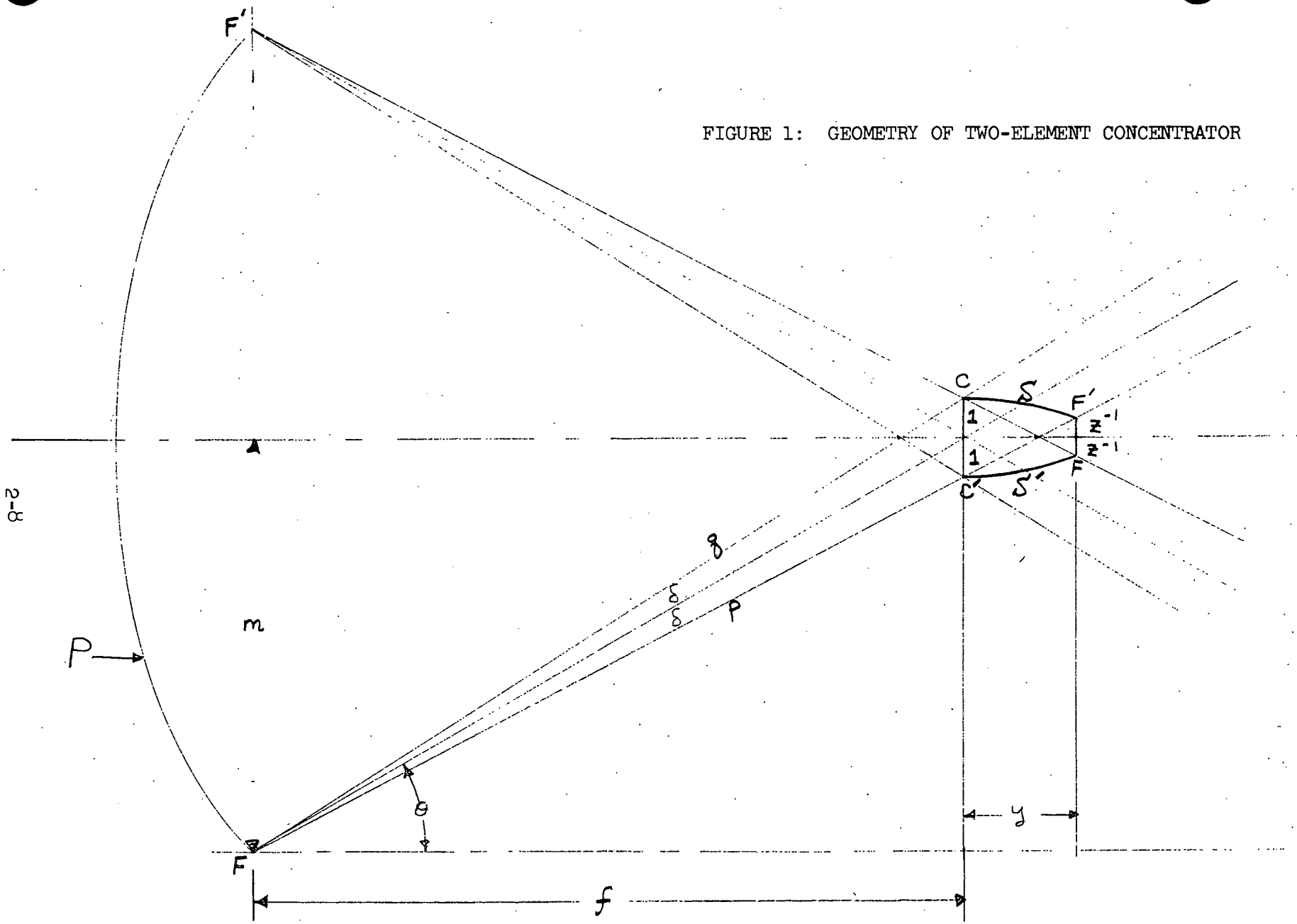

FIGURE 1: GEOMETRY OF TWO-ELEMENT CONCENTRATOR

TABLE I: PARAMETERS OF OPTIMIZED CONCENTRATORS

δ	θ	m	z	y	f	M	Mp	Mw	Yw
0.25°	9.36°	36.79	6.15	7.25	223.1	220.0	113.6	229.2	8238
0.40°	10.95°	26.71	5.26	6.39	138.1	135.4	70.6	143.2	3708
0.64°	12.81°	19.35	4.51	5.67	85.1	82.8	43.8	89.5	1661
1.0°	14.86°	14.21	3.89	5.10	53.6	51.5	27.7	57.3	770
1.6°	17.38°	10.21	3.35	4.60	32.6	30.8	16.9	35.8	339
2.5°	20.16°	7.42	2.90	4.23	20.2	18.6	10.5	22.9	153
4.0°	23.55°	5.26	2.50	3.94	12.1	10.6	6.19	14.3	65.2
6.4°	27.48°	3.70	2.15	3.80	7.11	5.81	3.51	8.97	26.8
10°	31.73°	2.62	1.87	3.85	4.24	3.03	1.92	5.76	10.8

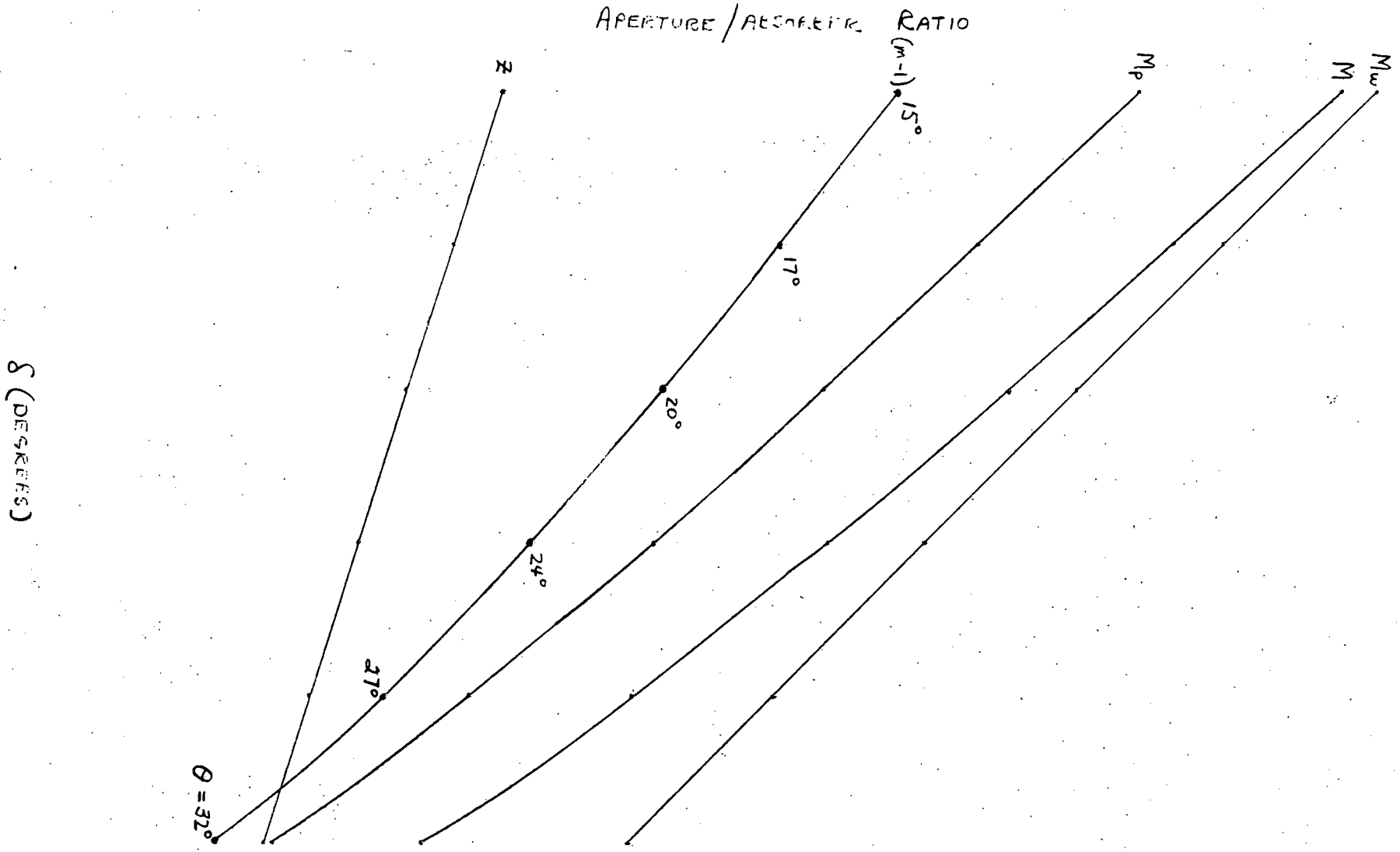

FIGURE 2: PERFORMANCE OF COMPOUND CONCENTRATORS

TABLE II: PARAMETERS OF OFF-OPTIMUM CONCENTRATOR DESIGNS

Designs for $\delta = 1°$:

θ	m	z	y	f	M
5°	4.98	11.5	15.5	56.9	45.6
10°	9.80	5.76	7.41	55.6	50.7
15°	14.3	3.86	5.05	53.5	51.5
20°	18.4	2.92	3.69	50.6	50.9
25°	22.0	2.37	3.05	47.1	49.6
30°	24.8	2.00	2.60	43.0	47.6
35°	26.9	1.74	2.25	38.5	45.2
40°	28.2	1.56	1.96	33.6	42.3
45°	28.7	1.41	1.71	28.7	39.1

Designs for $\theta = 30°$ ($z = 2.00$, $y = 2.60$):

δ	m	f	M	M/Mw
0.25°	99.2	171.9	196.5	0.86
0.40°	62.0	107.4	122.1	0.85
0.64°	38.8	67.1	75.5	0.84
1.0°	24.8	43.0	47.6	0.83
1.6°	15.5	26.9	29.0	0.81
2.5°	9.94	17.2	17.9	0.78
4.0°	6.22	10.8	10.4	0.73

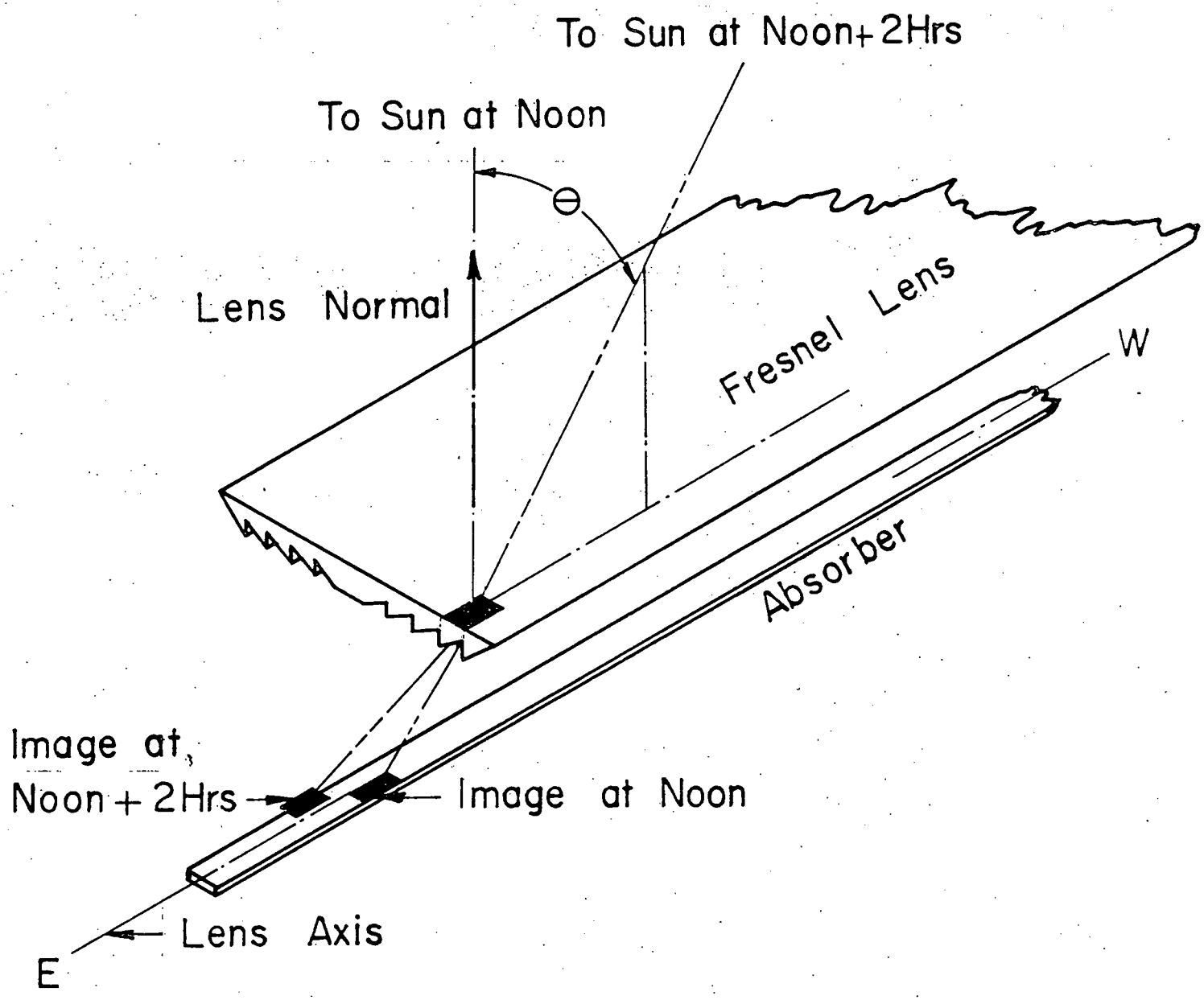

FIGURE 3: IMAGE MOVEMENT IN LINEAR FRESNEL LENS

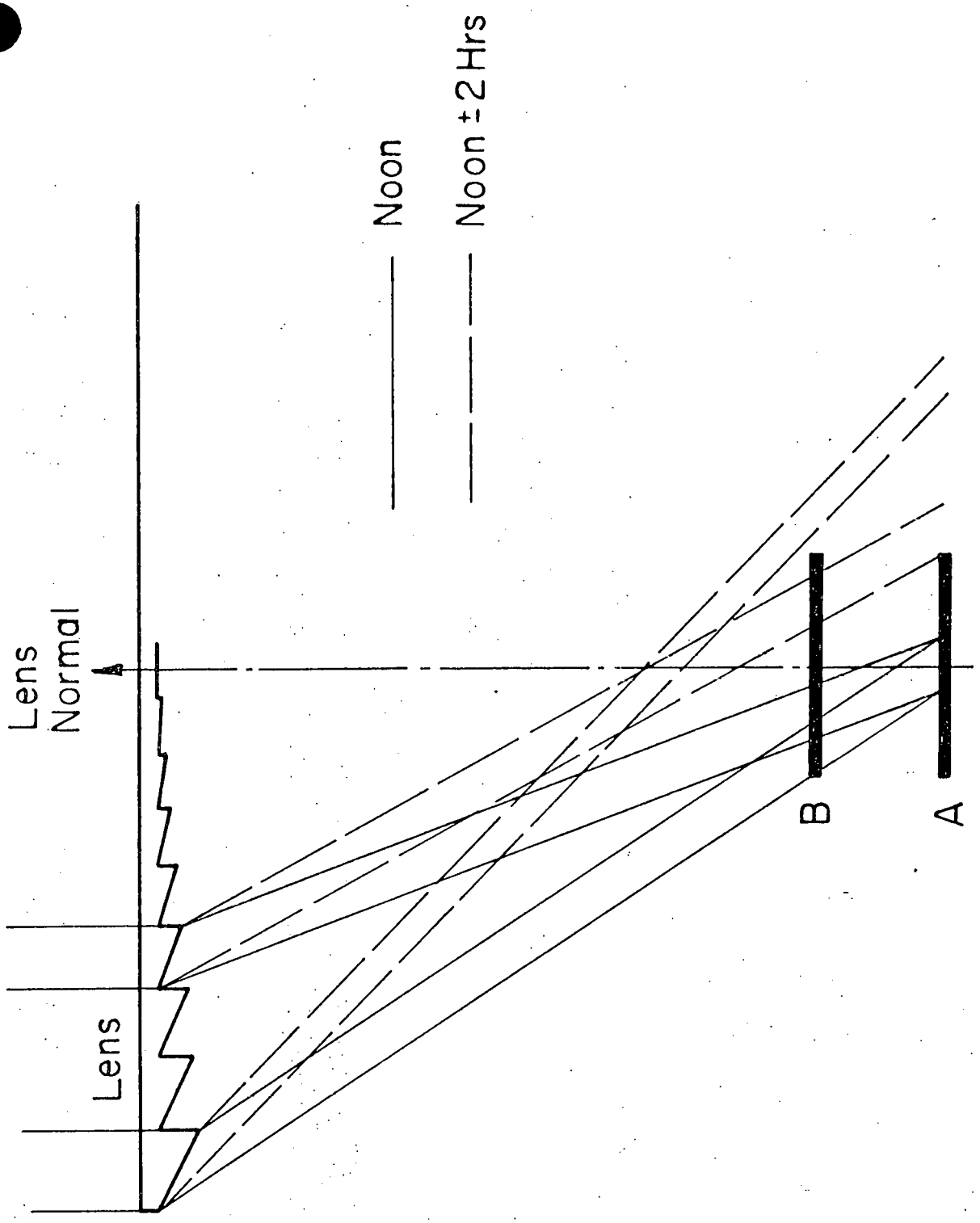

FIGURE 4: RAY TRACING OF LINEAR FRESNEL LENS

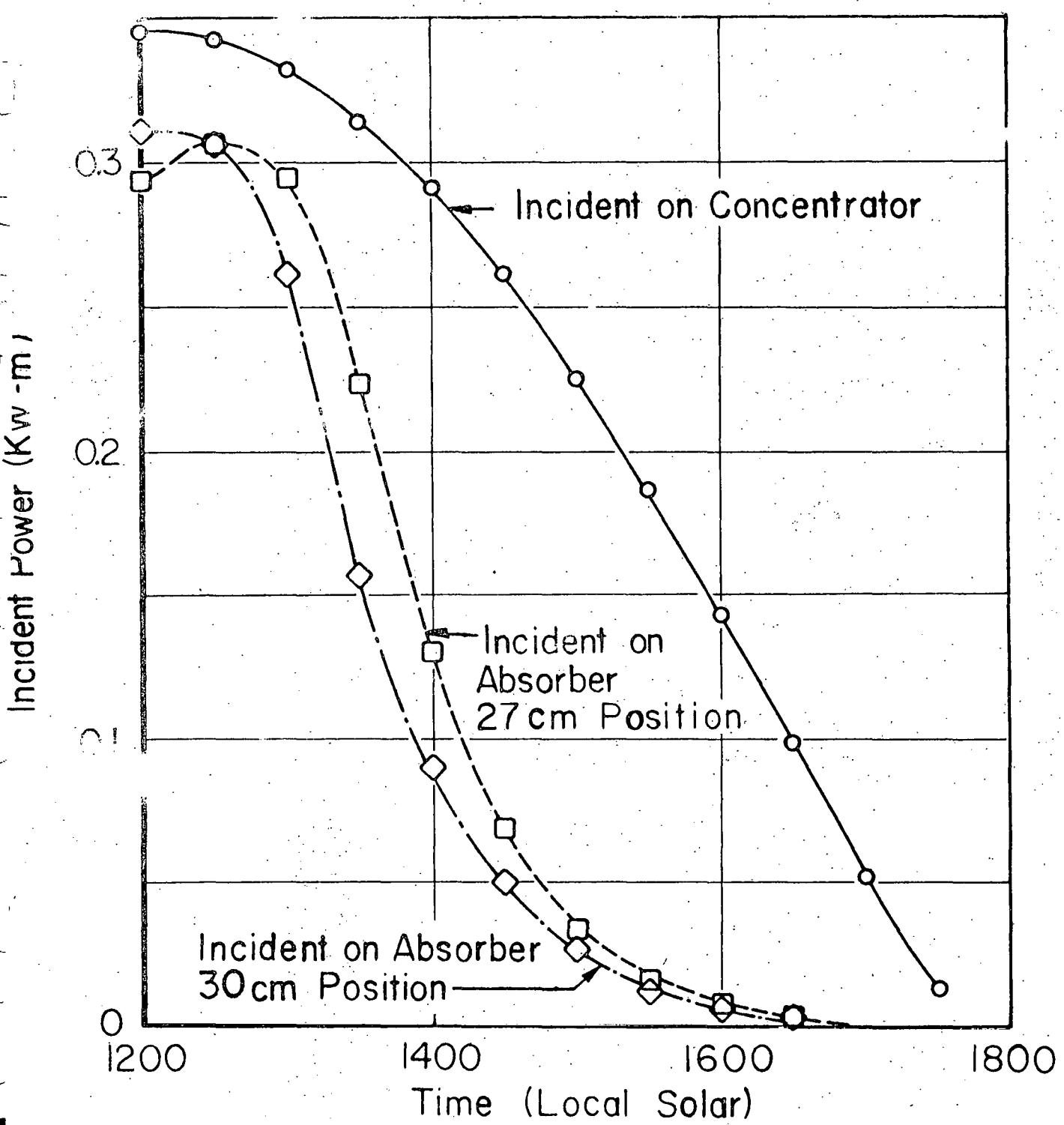

FIGURE 5: EFFECT OF IMAGE MOTION ON SOLAR ENERGY COLLECTION

ABSORBER ILLUMINATION

One of the main problems encountered in the concentration of sunlight onto silicon solar cells is series resistance in the cells. Unless cells having very low resistance can be developed, concentration ratios will be severely limited. Concentration devices which produce non-uniform intensity distributions on the cell or absorber are particularly prone to this problem, since the local high intensity spots play the major role in determining cell resistance.

It is important, therefore, to determine the intensity distribution on each potential concentrator device. In the present study, which is concerned mainly with seasonally or daily adjusted concentrators (non-diurnally tracked), three systems have been analyzed. These are the parabolic trough (PT), the compound parabolic concentrator (CPC), and the combination system consisting of a parabolic trough as a primary concentrator with a CPC secondary concentrator (PTCPC). The results presented, although for perfect mirrors, do provide some interesting insight regarding their potential performance. Ray tracing techniques have been used to analyze the intensity distributions.

RAY TRACING

Discussed here are the concepts underlying the ray tracing analysis. Time did not permit the tracing of rays that undergo two or more reflections in the CPC but, as will be seen, this would not affect the conclusions extensively.

We adopt the notation displayed in Fig. 1. The rays from the outer edges of the solar disk (marked "inner" and "outer" ray in Fig. 1) that

intersect at a point on the mirror surface form a cone both before and after reflection. The focal plane, which is perpendicular to the axis of symmetry and passes through the focus of the parabola, intersects this cone in an ellipse which has a major axis of $(y_i - y_o)$, where y_i and y_o are both measured positive upwards along the y axis from the focal point, and a minor axis of $(2r \sin \phi_s)$. Here

$$\left.\begin{aligned} y_i &= \pm \frac{r \tan \phi_1 \sec \theta}{(1 + \tan \phi \mid \tan \theta \mid)} \\ y_o &= \mp \frac{r \tan \phi_2 \sec \theta}{(1 - \tan \phi \mid \tan \theta \mid)} \end{aligned}\right\} \text{for } |\theta| < 90°$$

$$\left.\begin{aligned} y_i &= \frac{\mp r \tan \phi_1 \sec \theta}{1 - \tan \phi_1 \mid \tan \theta \mid} \\ y_o &= \frac{\pm r \tan \phi_2 \sec \theta}{1 + \tan \phi_2 \mid \tan \theta \mid} \end{aligned}\right\} \text{for } |\theta| > 90°$$

where the top signs apply for $\theta > 0$ and the bottom signs for $\theta < 0$. Also, normally,

$$\phi_s = \phi_1 = \phi_2$$

is the half angle subtended by the sun (16 minutes of arc). The equation for this ellipse in terms of coordinates Z (measured along the focal line,

i.e., normal to the plane of Fig. 1) and y measured upward from the focal line in the focal plane is

$$\frac{Z^2}{a^2} + \frac{[y + \frac{y_o + y_i}{2}]^2}{b^2} = 1$$

where $a = r \sin \phi_s \sim r \phi_s$ and $b = |(y_o - y_i)/2|$

The intensity of radiation reaching the absorber at location y is given by:

$$I(y) = \int_{A_A} = \rho I_s \cos \theta dA_A / r^2$$

where I_s is the solar intensity reaching the aperture, A_A, and ρ is the reflectivity of the mirror surface. Here we have used r, the radical coordinate in the denominator, in place of

$$\sqrt{r^2 + \Delta Z^2}$$

where ΔZ is the axial displacement between the view point and the infinitesimal area dA_A, for reasons to be justified shortly. We have also set the cosine of the angle between the normal to dA_A and the departing ray equal to 1, as will soon be made apparent. In cylindical coordinates, $dA = \cos \gamma r d\theta dZ / \cos (|\theta| + \gamma - \pi/2)$ where, for the parabola, $r = 2f/(1 + \cos \theta)$. Gamma (γ) is the angle between the mirror surface at point r, θ and the x axis; i.e.,

$$\gamma = \frac{\pi}{2} - |\theta|/2$$

For a solar disk of constant intensity the integration over Z at a constant θ can be shown to yield

$$2a\sqrt{1-\frac{(y-\frac{y_o+y_i}{2})^2}{b^2}}$$

This stems from the fact that any one location on the absorber can see only the overlapping ellipses that result from points (for which θ = constant) that extend a distance of

$$Z = \pm a\sqrt{1-\{[y-(y_o+y_i)/2]/b\}^2}$$

on either side of a transverse plane through the view point on the absorber. Thus, the earlier assumptions that

$$r \simeq \sqrt{r^2+\Delta Z^2}$$

and that the cosine of the angle between the aperture normal at dA_A and the departing ray is equal to 1, are justified.

The intensity I(y) becomes

$$I(y) = 2\rho I_s \frac{a}{f}\int_{\theta_1}^{\theta_2}\sqrt{1-[(Y-\frac{Y_1+Y_1}{2})f/b]^2}\ \sin\gamma\ X$$

$$\sec(|\theta| + \gamma - \tfrac{\pi}{2})\cos\theta d\theta/r'$$

where we have used the nondimensional variables $Y = y/f$, $r' = r/f = 2/(1+\cos\theta)$. By performing this integration for various values of Y, the intensity distrubition in the focal plane can be obtained.

The Parabolic Trough

The result of applying the derivation of the previous section to a 45° rim angle parabolic trough is shown in Fig. 2. The local concentration ratio (i.e., local intensity on the absorber compared to the solar intensity at the mirror aperture) is shown as a function of the nondimensional distance $Y = y/f$. The present results differ substantially from those of Ref. 1 due to the fact that their analysis is for a sun that is represented by an infinite strip and not a disk, although they state that they are using a constant intensity disk. No shading of the mirror surface by the absorber has been considered here although further extensions could incorporate this factor.

Off-axis performance of the same trough is represented in Fig. 3 for 2.5° off-axis operation. This was analyzed using the previous ray tracing analysis but considering the rays from the sun to have two extremes represented by two different ϕ_1's for $\theta > 0$ and two different ϕ_2's for $\theta < 0$. This allowed the location of the ellipses to be determined above or below the axis of symmetry of the mirror.

Image quality for off-axis operation is seriously degraded. The spread and skewness of the intensity distribution increases as the rim angle increases. These results show that a 45° rim angle mirror used as (at most) a daily adjusted concentrator would provide a concentration of about 11.3 during any projected 2.5° north-south movement of the sun.

Non-uniformity of the image during any collection period is extreme. Such illumination patterns are tolerable for thermal systems but very undesirable for photovoltaic systems due to the series resistance problems mentioned previously.

The Compound Parabolic Concentrator

The operation of a CPC having an acceptance angle of 2.5° was analyzed for comparison with the parabolic trough. Figure 4 shows the schematic of the device. As pointed out elsewhere[2] the depth of such small acceptance angle "ideal" concentrators is extreme, necessitating large amounts of material for construction of the reflector. The ray tracing consisted of a modified version of that discussed previously. Since the absorber in this case is nearly in the focal plane (it is only 2.5° out of the focal plane), the integral given in Equation 1 was evaluated between a lower limit of $\theta = 90°$ and an upper limit of 175°. Only the intensity on the portion of the absorber for $y > 0$ was considered. The tracing did not properly trace rays that were reflected two or more times on their journey through the device. It did, however, trace these rays under the assumption that they would pass through the reflector surface unchanged on their second encounter with the surface.

Figure 5 shows the results of operating the CPC with its aperture perpendicular to the central rays from the sun. This amounts to using the device 2.5° off the axis of one of the parabolas that make up the reflective sides. Therefore, as in the case of the off-axis PT, two different ϕ_2's differing by 32 minutes of arc were used to trace the edges of the solar cone through its intersection with the focal plane.

The intensity distribution does not go to zero at the edges of the absorber due to the rays that would normally undergo two or more reflections but which were not allowed to do so. These "tails" were found to be quite wide, extending out on both sides of the absorber almost half the aperture width. In operation, the energy in this "tail" would, after suffering reflection losses, be distributed over the absorber area changing slightly the distribution on the absorber shown in Fig. 5.

An intensity distribution for operating the 2.5° acceptance angle CPC at the extreme of its acceptance is also shown in Fig. 5. A nearly symmetrical second half of the distribution (not shown) impinges on the reflector which adjoins the absorber at the peak of the intensity distribution. The angles may be such that some of this energy gets eventually to the absorber, but this was not investigated.

This device has a more uniform intensity distribution than the parabolic trough especially at normal incidence. However, approximately 500 times more material is required for the CPC than for a PT which would give rise to a significant cost penalty. Also, surface slope errors arising in manufacturing, combined with the long distances the rays must travel, would most probably give rise to significant losses.

PTCPC

We now investigate the intensity distribution for the PTCPC. The PT is assumed to have a rim angle of 20.2° (which corresponds to an aperture of 1.159f). The intensity distribution in the focal plane of this primary concentrator is shown in Fig. 6, for both on-axis and 2.5° off-axis operation. The distribution for off-axis use is clearly not as skewed as that shown for a 45° rim angle mirror in Fig. 3, due to the decreased rim angle.

The aperture of the CPC must therefore be at least 0.104f wide, and the acceptance angle must be at least 22.7°. Using these values, the depth of the CPC must be 0.172f and the absorber width 0.04f, where f is the focal length of the primary mirror.

The intensity distribution a distance of 0.172f behind the focal plane of the PT (i.e., in the plane of the absorber of the CPC) can be easily obtained by following the cone of rays from their intersection on the primary mirror surface at angle θ (see Fig. 1) on through their intersection with a plane located behind the focal plane. Figure 7 shows the geometry for such ray tracing. The extremes of the ellipse now cuts plane A at points B and C and giving a semi-major axis of

$$b = \frac{1}{2}\left|\{L[\tan(\theta + \phi_2) - \tan(\theta - \phi_1)] + y_i - y_o\}\right|$$

By sitting at one location in plane A, one can now sum up the contributions from ellipses for all possible θ's that overlap the viewing point, in much the same way as was done previously in the focal plane. Figure 8 shows the results of such a calculation for both on-axis operation and 2.5° off-axis operation. No shading of the primary concentrator by the CPC has been considered. The chosen secondary CPC would reflect the portions of this intensity distribution beyond $|y| = .02f$ onto an absorber located at $|y| \leq .02f$.

A schematic of the CPC for this design is shown in Fig. 9. Ray tracing to find the final intensity distribution on the absorber was carried out in the following way. First, all rays for on-axis operation were assumed to enter the CPC at the center of its aperture. As can be seen from Fig. 6,

this is a good, but not exact, approximation. Then, at 0.5° increments off the CPC centerline, rays were traced from the center of the aperture to both their intersection with the parabolic reflector (e.g., points A, B, C in Fig. 9) and with the plane of the absorber (points A', B' C' in Fig. 9). The reflected rays originating at the reflector were then traced until they intersected the absorber (points A", B", C" in Fig. 9). The rays striking the absorber directly (e.g., the ray striking point D in Fig. 9) do not undergo reflection. This ray tracing, done by computer, thus provided information on how to shift the intensity distribution for $|y|>0.02f$ in Fig. 8 onto the absorber located at $|y|\leq 0.02f$. That is, points A', B', C' map onto points A", B", C". In shifting the intensity distribution, the magnitude has to be increased or decreased by the ratio of $\cos \Omega"/\cos \Omega'$ where Ω' is the angle of incidence of the rays at the absorber plane if they were allowed to pass through the reflector (e.g., at points A', B', C') and $\Omega"$ is the angle of incidence of the rays at the point where they strike the absorber (e.g., at points A", B", C"). The extremely small difference in path lengths has been ignored.

The intensity distribution was then reconstructed by hand using the mapping and angle of incidence results obtained from the computer. Figure 10 shows the reconfigured distribution. It is more uniform than either the PT or the CPC used as single element concentrators. Neither reflectivity losses nor shadowing of the primary mirror by the CPC has been considered. The intensity in the "wings" (i.e., points $|y|>0.02f$) of the distribution are, in reality, reduced in magnitude by (1-R), where R is the reflectivity, before being reflected to the absorber. Shading can be accounted for by

subtracting out the intensity distribution due to the shaded apex area of the primary mirror, for this design $\pm$ 2.86° on either side of the axis of symmetry through the apex and the focal point of the PT primary. Figure 11 shows the results of considering shading for the design considered here. The distribution is more uniform than that shown in Fig. 10.

An investigation of the off-axis performance of this PTCPC was started but time did not permit its completion. These studies did show, however, (a) that double reflection does occur for some rays, and (b) that some local high intensity points can be expected to occur.

References

1. Kamal-Eldin Hassan and Mohamed Fawzi El-Refaie, "Theoretical Performance of Cylindrical Parabolic Solar Concentrators," Solar Energy 15, 219 (1973)

2. Ari Rabl, "Comparison of Solar Concentrators," Report SOL 75-02, Argonne National Laboratory, Argonne, IL

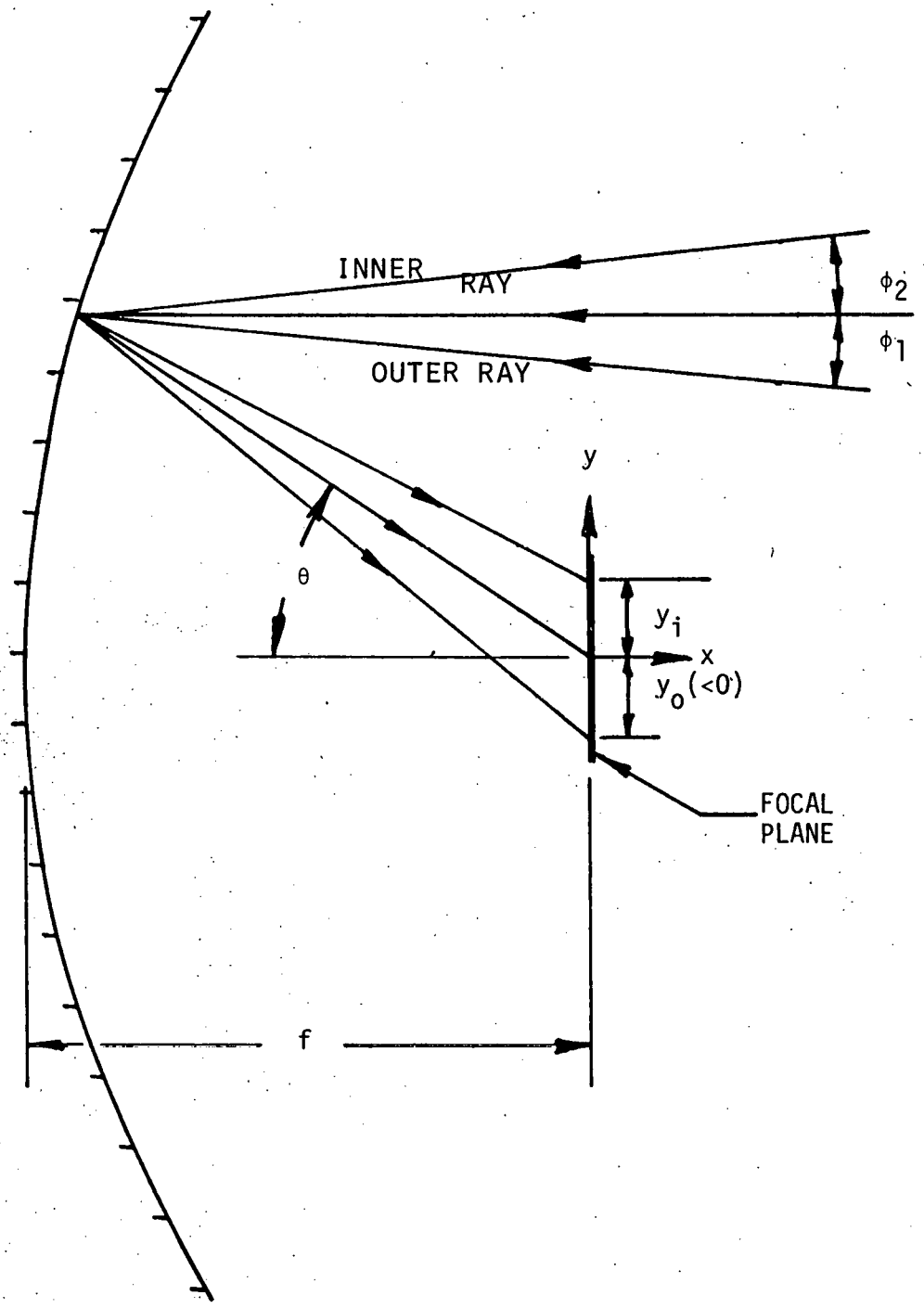

FIG. 1. PARABOLIC TROUGH GEOMETRY

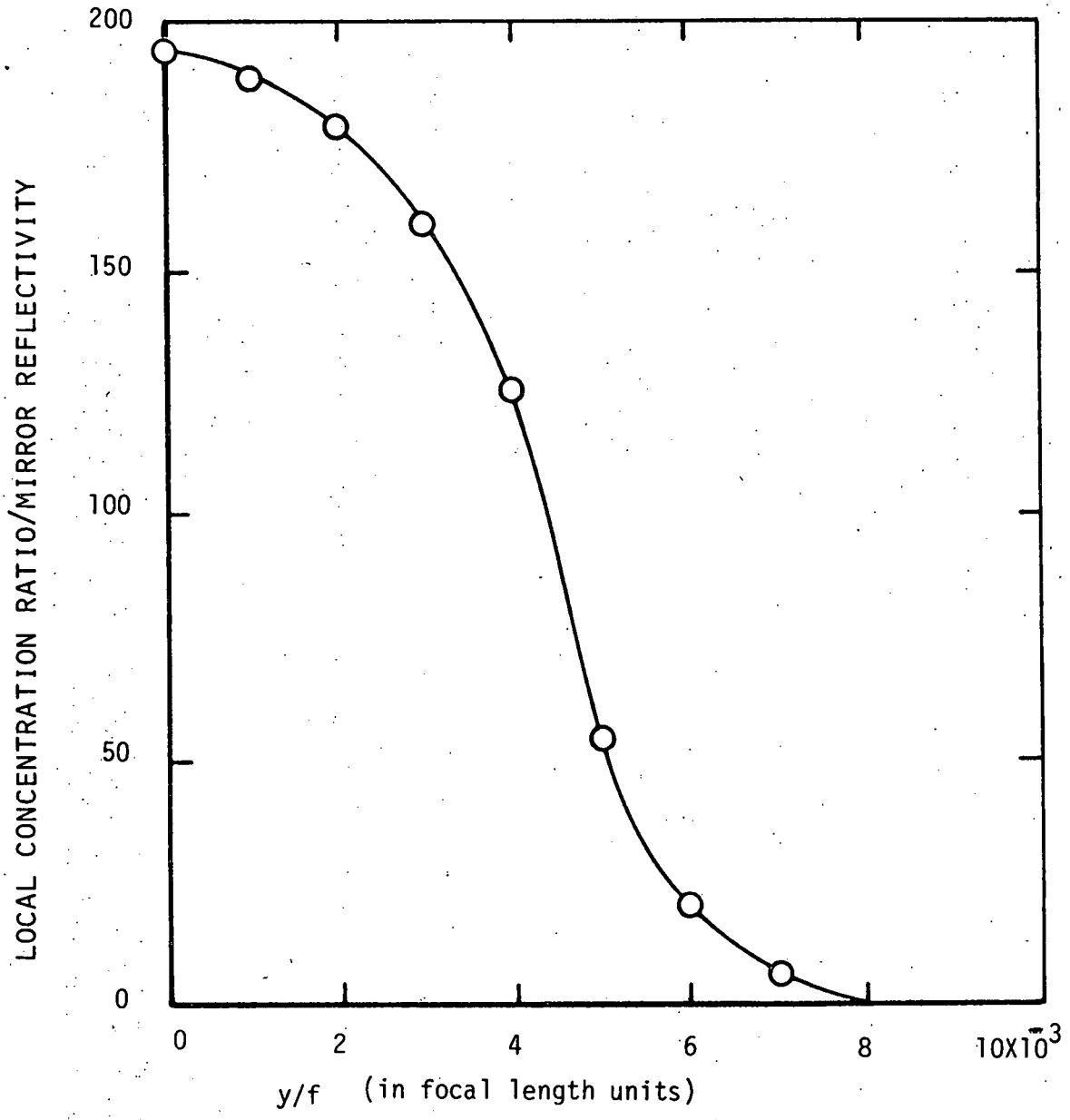

FIG. 2. LOCAL CONCENTRATION RATIO DISTRIBUTION IN THE FOCAL PLANE OF A PERFECT PARABOLIC TROUGH OF RIM ANGLE 45°, OPERATED ON-AXIS.

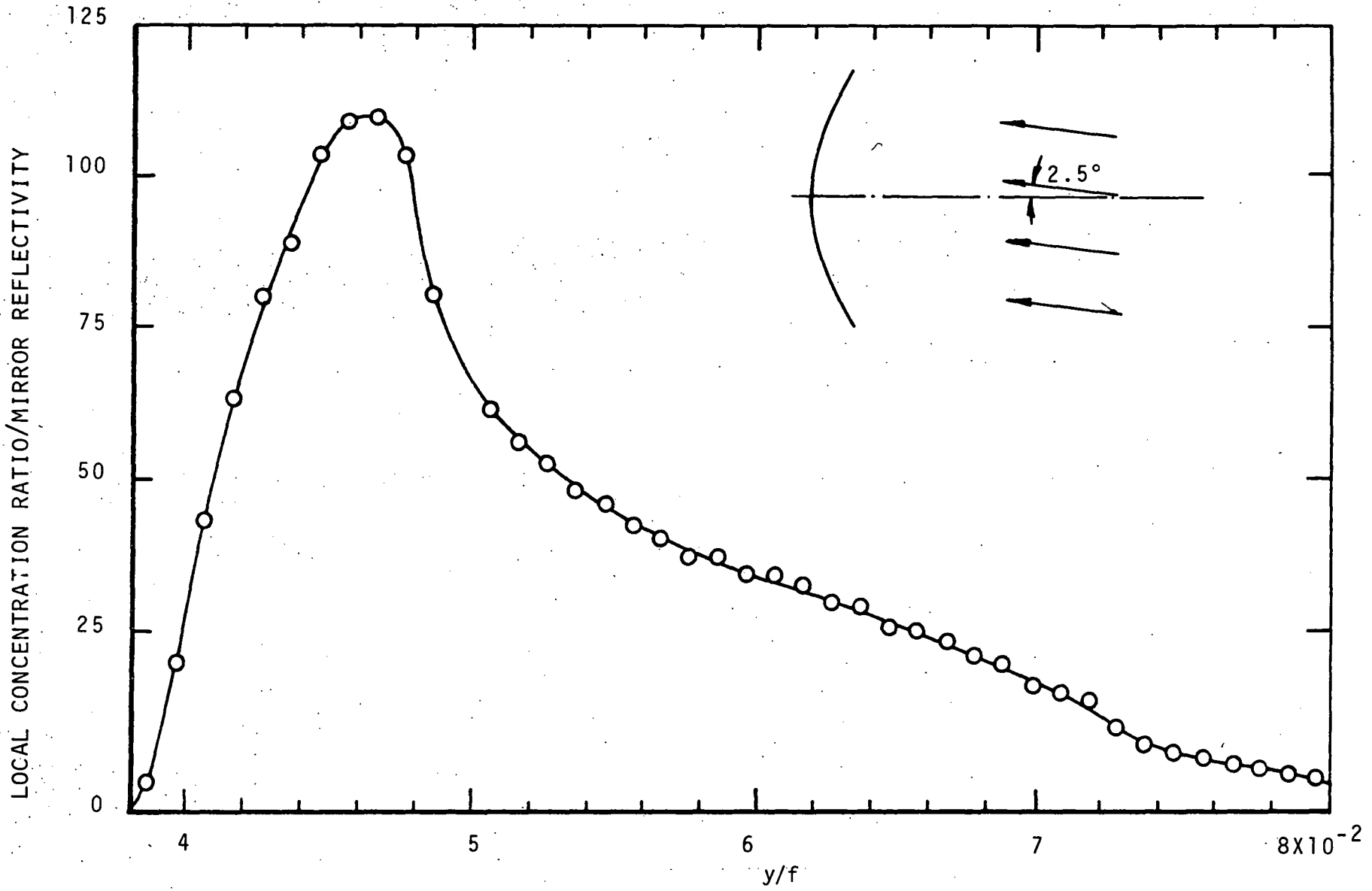

FIG. 3. LOCAL CONCENTRATION RATIO DISTRIBUTION IN THE FOCAL PLANE OF A PERFECT PARABOLIC TROUGH OF RIM ANGLE 45°, OPERATED 2.5° OFF-AXIS

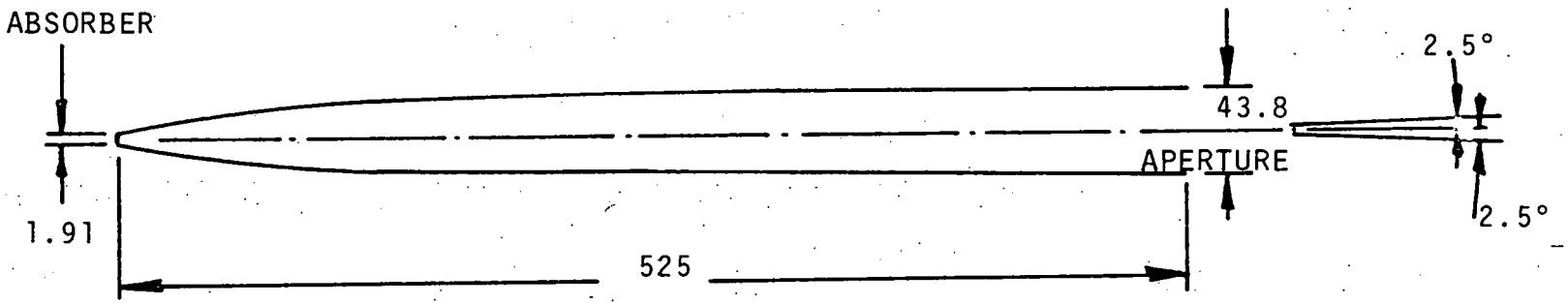

FIG. 4. SCHEMATIC OF 2.5° ACCEPTANCE ANGLE CPC. DIMENSIONS ARE IN UNITS OF THE FOCAL LENGTH OF THE PARABOLAS THAT MAKE UP THE REFLECTING SIDES

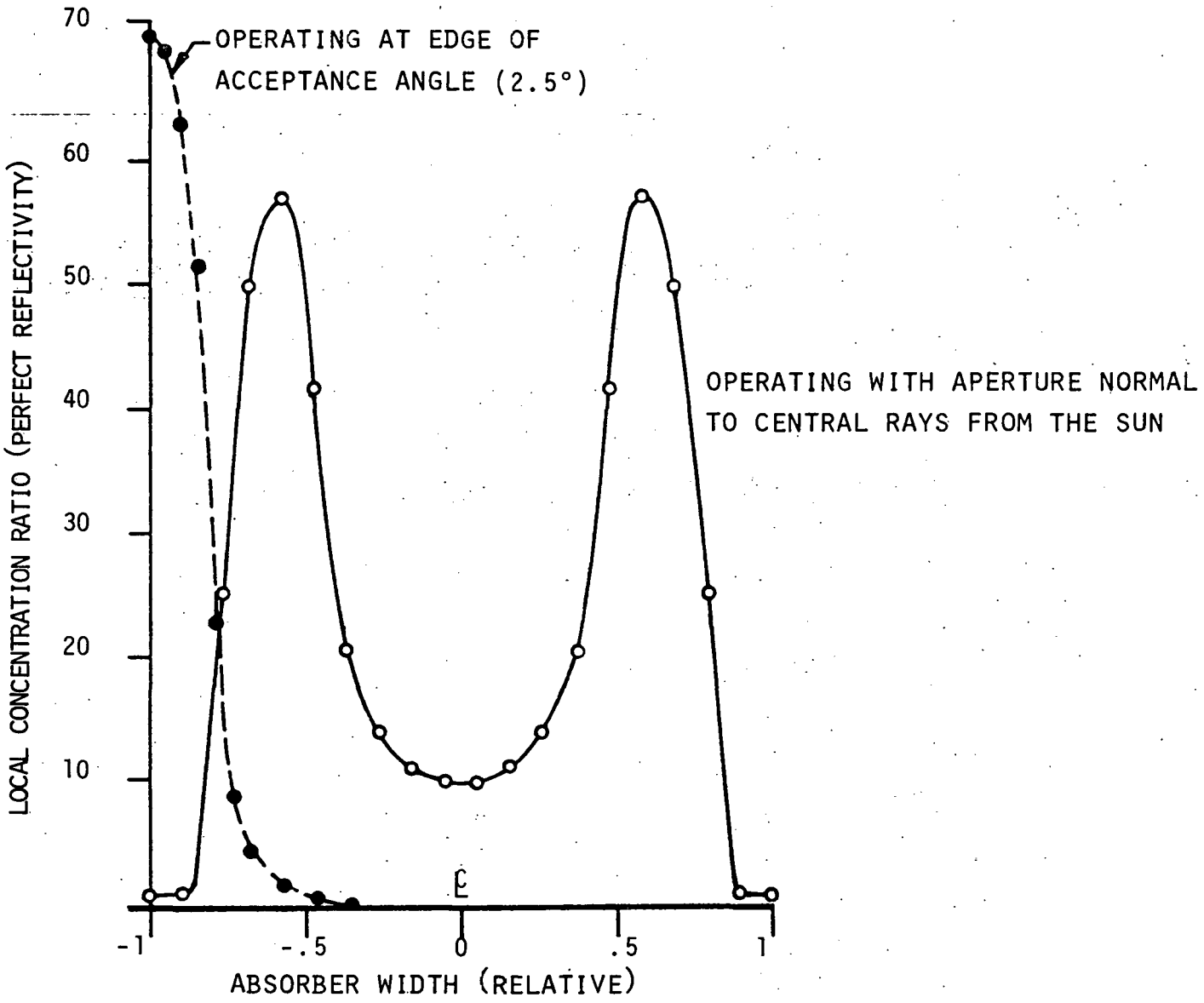

FIG. 5. LOCAL CONCENTRATION RATIO DISTRIBUTION FOR A 2.5°ACCEPTANCE ANGLE CPC

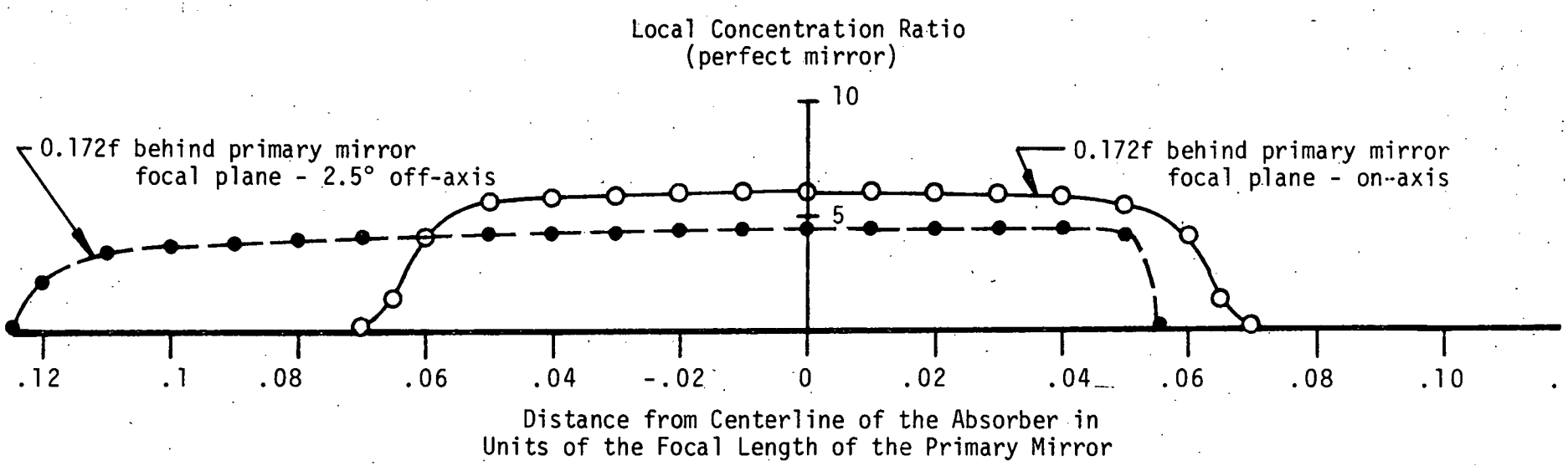

FIG. 6. INTENSITY DISTRIBUTION IN A PLANE PARALLEL TO BUT 0.172F BEHIND THE FOCAL PLANE OF A 20° RIM ANGLE PARABOLIC TROUGH

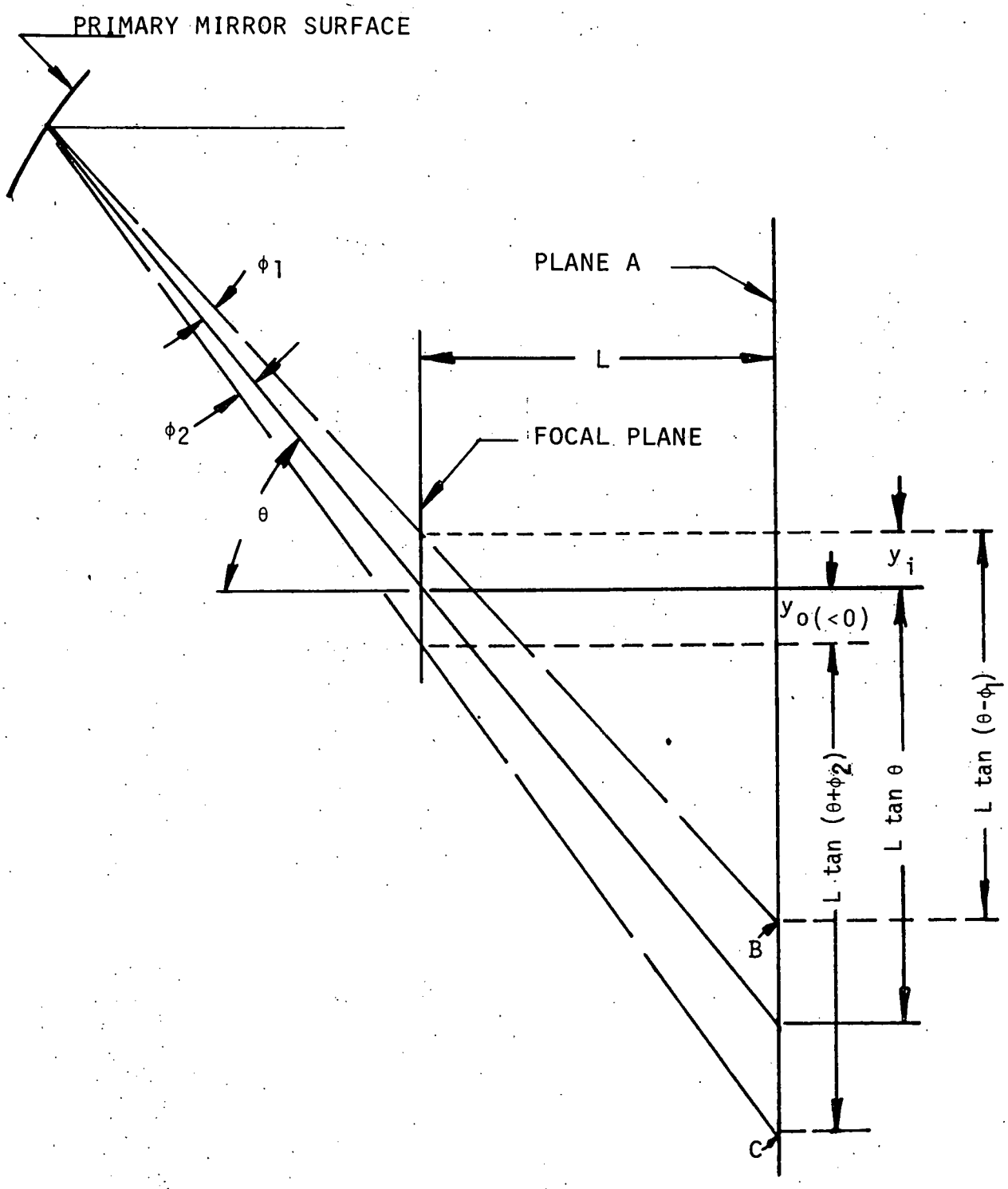

FIG. 7. SCHEMATIC FOR DEFOCUSSED USE OF THE PT

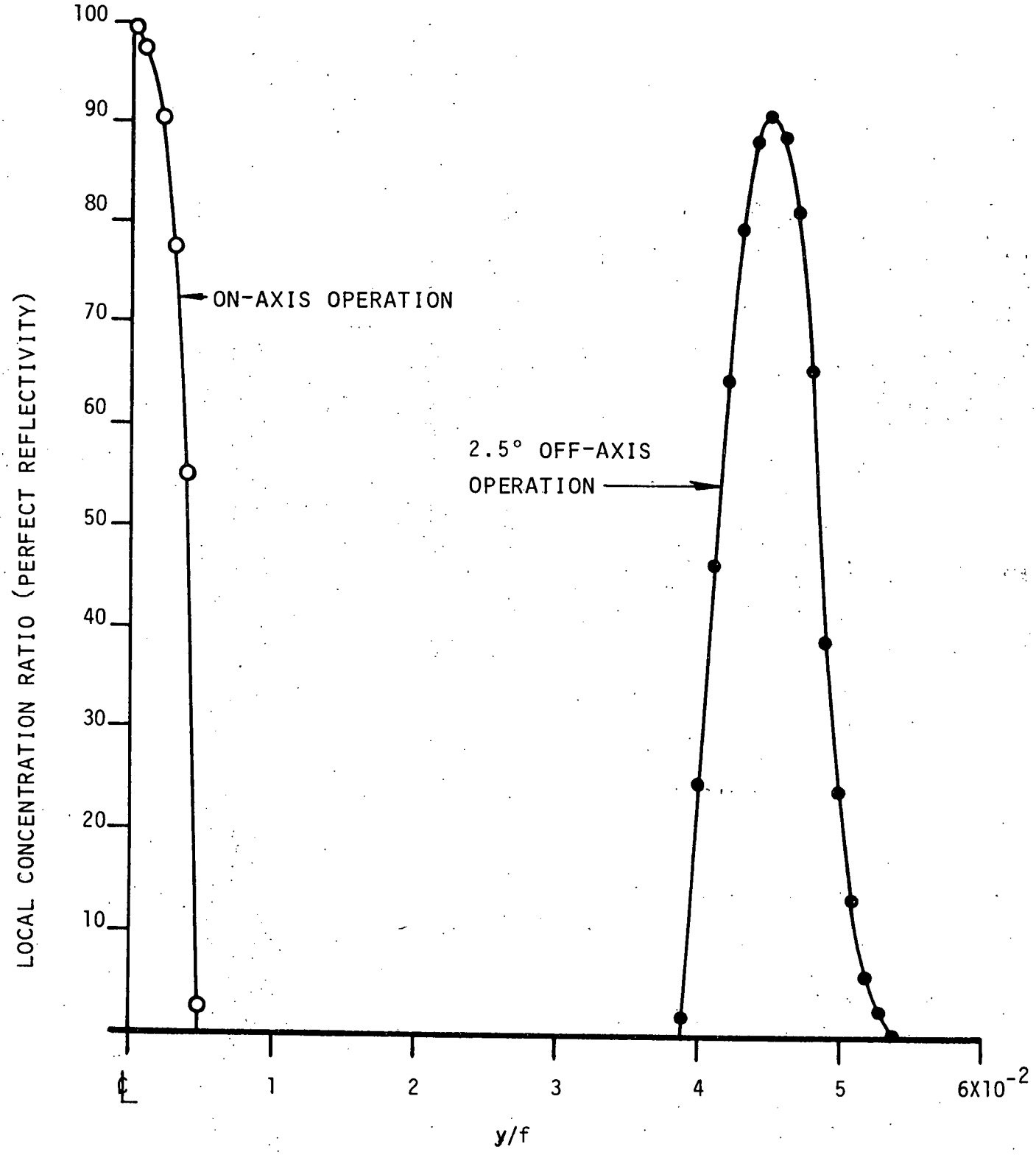

FIG. 8. LOCAL CONCENTRATION RATIO DISTRIBUTION IN FOCAL PLANE OF 20° RIM ANGLE PARABOLIC TROUGH

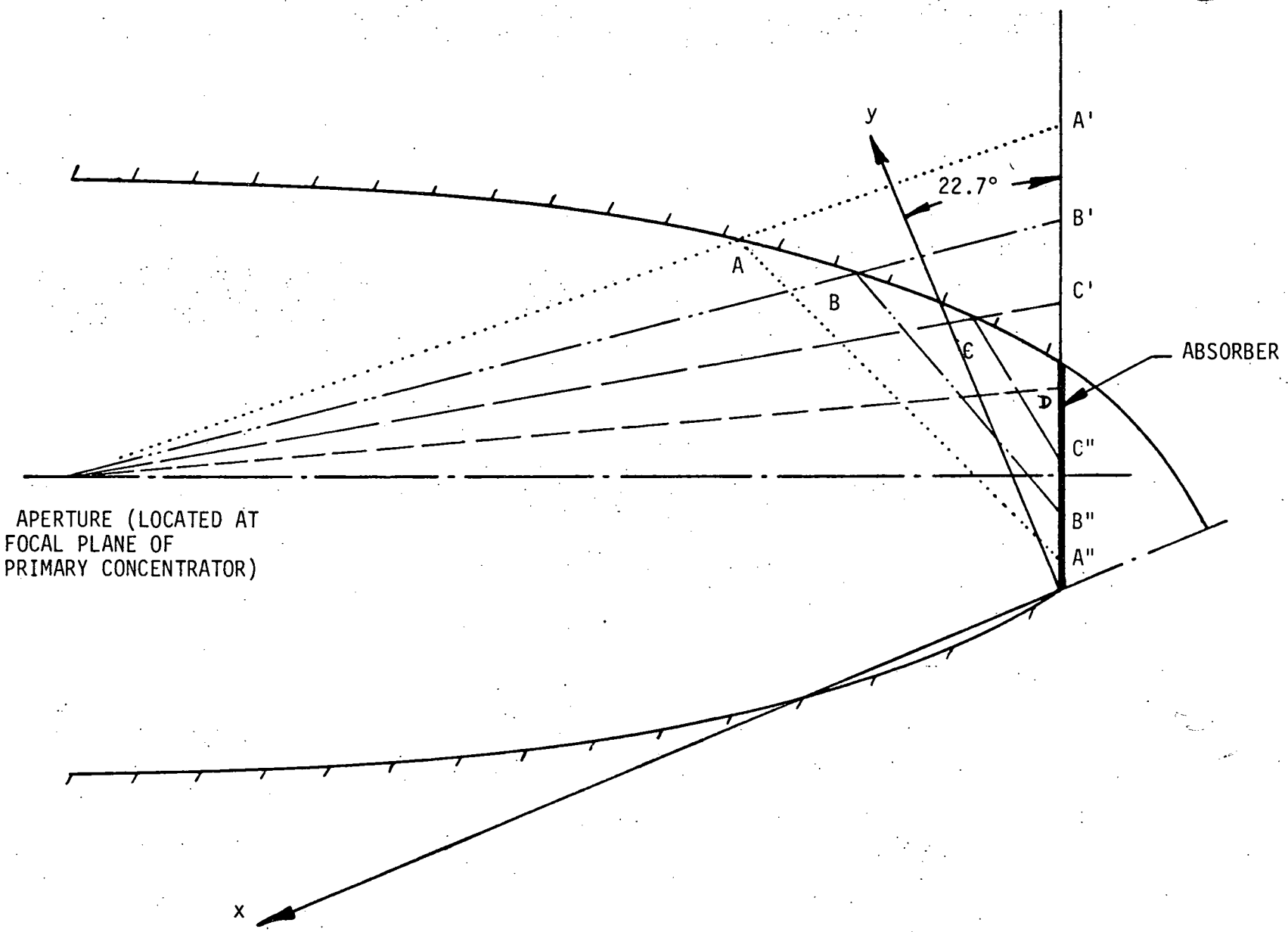

FIG. 9. SCHEMATIC OF CPC USED IN THE RAY TRACING STUDIES WITH THE 20° RIM ANGLE PRIMARY CONCENTRATOR FOR ON-AXIS OPERATION

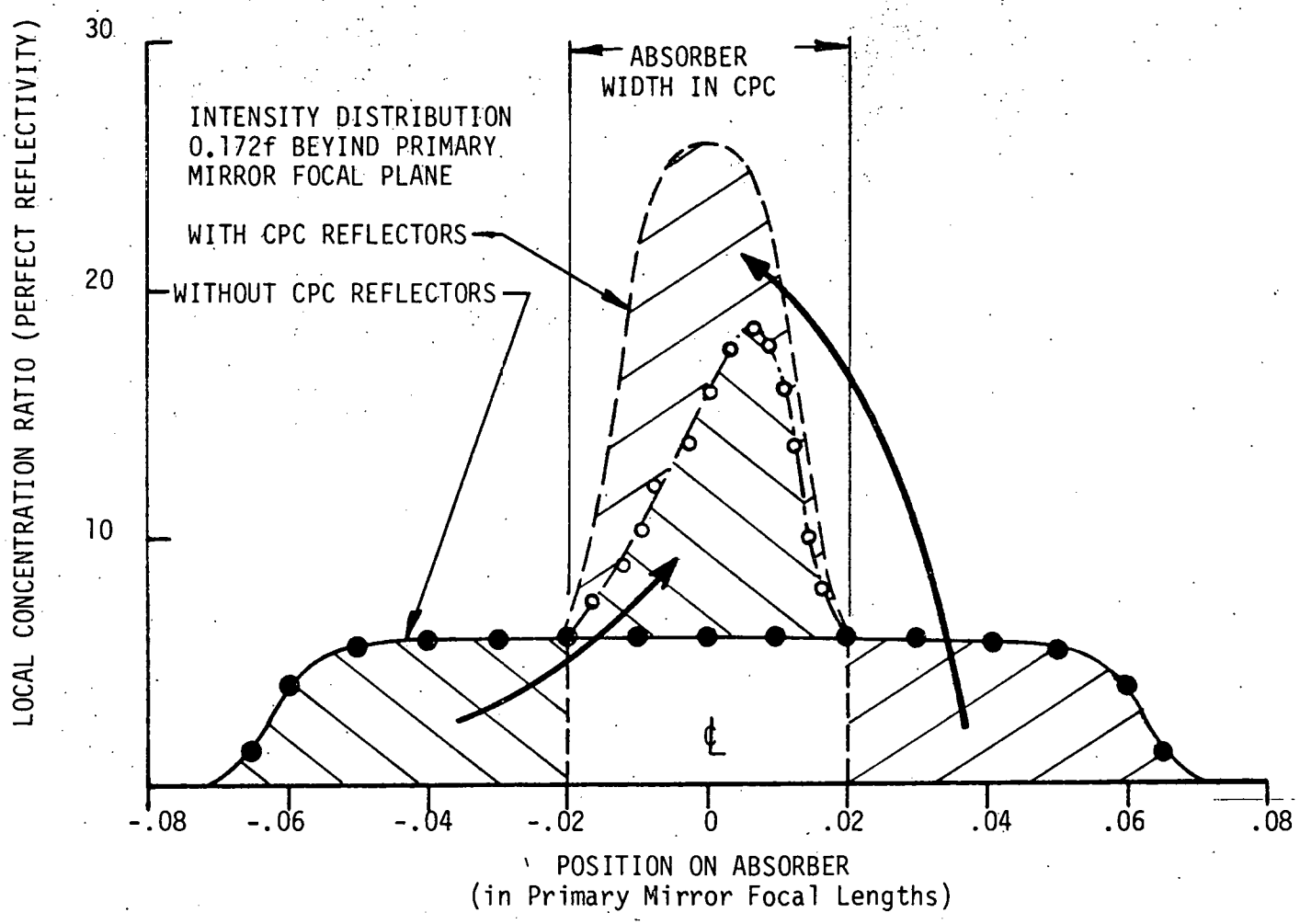

FIG. 10. LOCAL CONCENTRATION RATIO DISTRIBUTION ON ABSORBER OF PTCPC

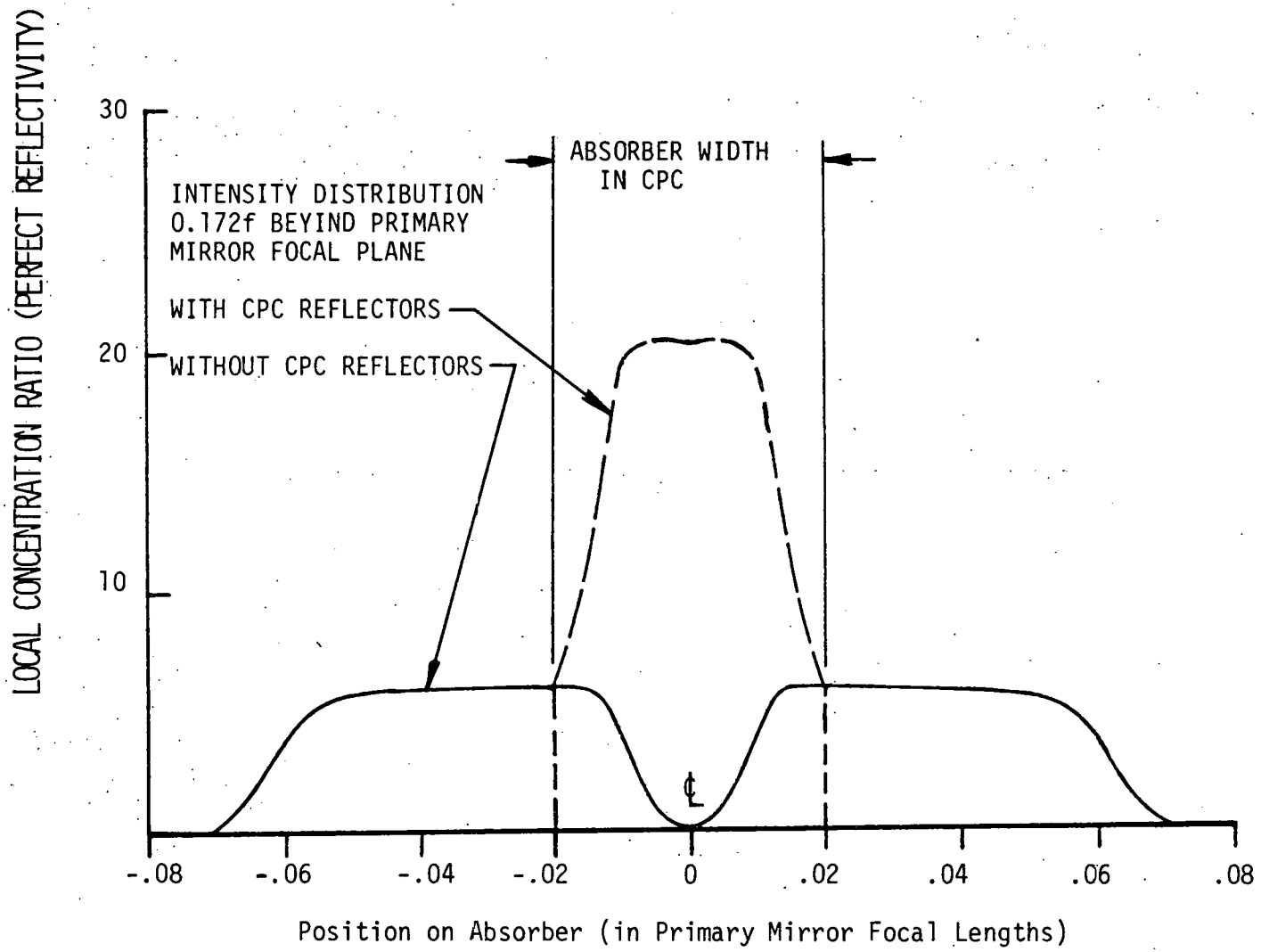

FIG. 11. LOCAL CONCENTRATION RATIO DISTRIBUTION ON ABSORBER OF PTCPC CONSIDERING SHADING OF PRIMARY MIRROR BY THE CPC

COOLING CONSIDERATIONS

INTRODUCTION

A preliminary examination of the potential effectiveness of techniques for passive cooling to ambient air and forced water cooling of solar cells coupled with CPC concentrators has been performed. Effective thermal conductance values for several illustrative alternative configurations have been calculated. These results, along with an indication of their relationship to cell output over a range of irradiation levels, are described and discussed in the following paragraphs.

A simple model combining cooling system and cell performance characteristics can be developed if it is assumed that the solar irradiation and heat rejection are uniform over the absorber surface, and that the heat rejection rate is proportional to the temperature difference between the cell and ambient air for passive cooling, or between cell and coolant for active cooling [1]. In addition, it is assumed that the cell efficiency decreases linearly with temperature. Such a model, though quite simple, is also quite useful for preliminary assessment of cooling schemes and basic system simulation.

The above noted assumptions, combined with an energy balance on the absorber, lead to the following result for cell power output, P, or cell efficiency, η, in normalized form:

$$\frac{P}{P_o} = \frac{\eta}{\eta_o} = \frac{1 - \left(\frac{\alpha q_s \beta_o}{K_e}\right)}{1 - \left(\frac{\alpha q_s \beta_o}{K_e}\right)\left(\frac{A_c}{A_a}\right)\left(\frac{\eta_o}{\alpha}\right)} \qquad (1)$$

Here P_o and η_o are the power output and cell efficiency which would exist if the cells were at the ambient air or inlet coolant temperature, T_o. q_s is the solar irradiation seen by the absorber, A_c/A_a is the fractional cell coverage of the absorber, and α is its effective solar absorptance. K_e is the effective thermal conductance, defined as the heat rejection rate per unit absorber area per unit temperature difference between cell and ambient for passive cooling or between cell and coolant inlet for active cooling. The defining equation for K_e is $Q = K_e A_a (T_c - T_o)$. β_o is the fractional decrease in cell efficiency per unit increase in cell temperature, given by $\beta_o = (T_c^* - T_o)^{-1}$ where T_c^* is the cell temperature at which the efficiency drops to zero ($\sim$ 270°C for silicon cells).

For passive cooling schemes, both cell temperature, T_c, and ambient temperature, T_o, may be considered uniform over the absorber area. In such a case K_e will be identical to the local thermal conductance, which ordinarily may be considered uniform over the absorber area.

For active cooling, T_o represents the coolant inlet temperature. As the coolant flows past the heat transfer surface, its temperature, along with the local cell temperature will rise. For such a case T_c represents the mean cell temperature and K_e may be calculated from

$$\frac{K_e}{K} = \frac{1}{1 + \frac{KA_a}{2\dot{m}c}} , \qquad (2)$$

where $\dot{m}$ and c are the mass flow rate and specific heat of the coolant fluid. Here K is the local thermal conductance, referred to absorber area, for

heat transfer across the local temperature difference between cell and coolant. Equation (2) is valid for uniform heat rejection and uniform K over the absorber area. An additional condition is that the coolant temperature rise along its flow path be linear. This is an excellent approximation for coolant flow along a duct such as might be used for active cooling of cells coupled with a two-dimensional CPC.

A generalized plot of Equation (1) is shown in Fig. 1. Note that the parameter $A_c\eta_o / A_a\alpha$ is secondary in its influence on P/P_o.

Based on Equation (1), the effective thermal conductance vs. solar irradiation is shown in Fig. 2 for silicon cells, with output at various fractions of that for the limiting case of cells operating at ambient air or coolant inlet temperature.

Cell output per unit absorber area as a function of solar irradiation, again for silicon cells, is shown in Fig. 3 for a range of values of effective thermal conductance. The limiting case of infinite thermal conductance corresponds, of course, to $P = P_o$. For a given thermal conductance the power output passes through a maximum as the irradiation level is increased. It may be shown [1] that to a good approximation this maximum is given by $P_{max} = 0.5\ P_o$, indicated by the dashed line in Fig. 3.

PASSIVE COOLING

For initial assessment of potential performance for passive cooling of solar cells coupled with a two-dimensional CPC, three configurations were selected as shown in cross-section in Fig. 4. Configuration A is a basic CPC with no extended surfaces added for augmentation of heat transfer, except for the reflector surfaces which are already inherent to the CPC

design. Configurations B and C include longitudinal fins. The material assumed is aluminum alloy 6063-T5, with a thermal conductivity of 209 W/m °C at 25°C. Each of these configurations could presumably be manufactured by an extrusion operation. The particular fin designs indicated are not optimized in any particular sense, but were selected as reasonable for illustrative purposes and because some empirical information on convective heat transfer coefficients for these finned arrays was available [2,3]. Since the CPC is to be considered for use with a primary reflecting surface, a constraint used in the selection of arrangements for heat transfer augmentation surfaces is that they should not block incoming solar radiation from reaching the primary concentrator to an extent greater than the blockage caused by the basic CPC.

For evaluation of effective thermal conductance, K_e, under natural convection conditions the inverted vertical orientation shown in Fig. 4 was assumed on the basis that the CPC would be the secondary concentrator in a system whose major axis is east-west. The vertical orientation approximates that which would occur for summertime operation when ambient temperatures are highest.

For considering forced convection conditions, that is the effect of the presence of wind, cross-flow normal to the axis of the CPC was assumed as a reference condition.

Even for such a relatively simple geometry as flow in a circular tube the prediction of convective heat transfer is usually considered to have an associated uncertainty of about $\pm$ 20%. For the more complex geometric configurations under consideration here, it must be recognized that the

uncertainties are even larger, especially when coupled with the random nature of actual wind patterns. Therefore, predictions of effective thermal conductance values for such cases must be regarded as subject to verification by system tests under field conditions.

In the computational model utilized it was assumed that the temperature of the absorber base plate into which the heat initially flows (dimension "a" in Fig. 4) was uniform and equal to the cell temperature. For passive cooling the thermal resistance across the adhesive bond between cell and base plate will be at least an order of magnitude less than that between the base plate mounting surface and ambient. Individual heat transfer coefficients were assumed uniform over each surface of each type of element (i.e., reflector wall, base plate extention, finned array), but temperature variations along these elements were accounted for by calculation of an appropriate fin efficiency. In calculating these fin efficiencies temperature gradients across the thickness of the elements were neglected.

The contribution to the net heat rejection rate due to infrared radiation was included. Under natural convection conditions it accounts for over 50% of the total heat rejection. It was not linearized, but calculated according to the Stefan-Boltzmann fourth power law. The radiation surrounds temperature was taken as 25°C for these calculations. All surfaces were assumed to have an infrared emittance of 0.9 (the apparent emittance in the case of the finned surfaces). This value would not be appropriate for the inner surfaces of the reflector walls, if these were first surface mirrors, but was utilized for them anyway to simplify the computational model. Since these surfaces see each other and the absorber surface as well

THIS PAGE

WAS INTENTIONALLY

LEFT BLANK

and the average temperature level continues to drop further below the cell temperature level.

The effect under calm air conditions of adding finned surfaces is illustrated in Fig. 6, while a similar comparison for the case of a 3 m/s wind is shown in Fig. 7.

WATER COOLING

Figure 8 shows two configurations for forced water cooling. Assumed flow conditions and the results of evaluation of effective thermal conductance values are also summarized. In these cases, all heat rejection was assumed to occur to the cooling water. Here the effective thermal conductance is essentially independent of the absorber width or size of the associated CPC. After determination of the local conductance, K, assumed uniform along the absorber, K_e was computed from Equation (2). In determination of K standard convective heat transfer correlations for turbulent flow in channels were utilized. K also includes the effect of the cell/heat-sink bond thermal resistance assumed to be 0.25 $m^2 \cdot °C/kW$. The effect of nonuniform heat input around the periphery of the flow channels was accounted for by utilizing an equivalent fin efficiency applied to those portions of the channel periphery not directly opposite the cell mounting surface.

EFFECTS OF COOLING SCHEME ON CELL OUTPUT

Utilizing some of the results for effective thermal conductances discussed in the preceeding paragraphs, Fig. 9 was constructed as an illustration of a comparison between passive cooling and water cooling as it affects output for silicon cells coupled with a CPC. Cell output as a fraction of that for cells at ambient temperature is plotted as a function of irradiation

level. Note that if one sun is taken as 1 kW/m^2, the scale on the abscissa may be interpreted as an energy concentration ratio. These results are based on Equation (1) with $\alpha = 0.8$, $\beta_o = .0041\ °C^{-1}$, and $A_c\eta_o/A_a\alpha = 0.15$.

The solid curves represent passive cooling for configuration C with a wind speed of 3 m/s, for a range of absorber widths. The points on these curves represent relative operating points corresponding to primary collector surface apertures fixed at the several values indicated. If an initial design constraint is a fixed primary aperture width, e.g., 1m, then performance is similar for a range of absorber widths. This illustrates the point that while effective thermal conductance values are smaller for the larger absorber widths, comparative performance with a fixed primary aperture will be somewhat better since the irradiation level to be accommodated will be smaller.

The dashed curves represent water cooling for cases B and C as summarized in Fig. 8. The curve for cases A and D, if shown, would fall between those shown for B and C. It should be noted that for water cooling with a recirculating system an additional temperature drop between coolant and ambient would be required for final heat rejection. The dashed curves are adjusted for a difference of 25°C between the coolant inlet temperature and ambient air. This difference should be large enough to allow for natural draft dry cooling for final heat rejection, eliminating the need for fan power. There is still, however, a power requirement for water circulating pumps, but this should be relatively small.

It appears from this comparative illustration that from the standpoint of cell output water cooling is the most advantageous, increasingly so

as irradiation levels become larger. However, passive cooling performance may be improved to some extent by optimizing, under field conditions, the height and aspect ratio of the straight longitudinal finned arrays considered here. A difficulty is that as fins are made higher and spaced more closely to gain surface area, local heat transfer coefficients tend to decrease due to adversely modified local flow patterns. Improved performance could unquestionably be achieved by the use of transverse strip fins or pin fins, but manufacturing costs would be increased over those for simple extrusion of longitudinal fins.

Final conclusions regarding passive vs. active cooling must also take into account the complex considerations of type of application, siting (e.g., what wind conditions exist during collection hours), relative costs, reliability, effects on overall system design, and system control during operation.

REFERENCES

1. L. W. Florschuetz, On Heat Rejection from Terrestrial Solar Cell Arrays with Sunlight Concentration, 11th IEEE Photovoltaic Specialists Conference, Phoenix, May 1975.

2. C.D. Jones and L.F. Smith, Optimum Arrangement of Rectangular Fins on Horizontal Surfaces for Free-Convection Heat Transfer, J. Heat Transfer, 92, pp. 6-10, Feb 1970.

3. Unpublished data recently obtained by J. Kidd, Mechanical Engineering, Arizona State University.

4. B. Beghart, Heat Transfer, 2nd Edition, McGraw-Hill, New York, 1971.

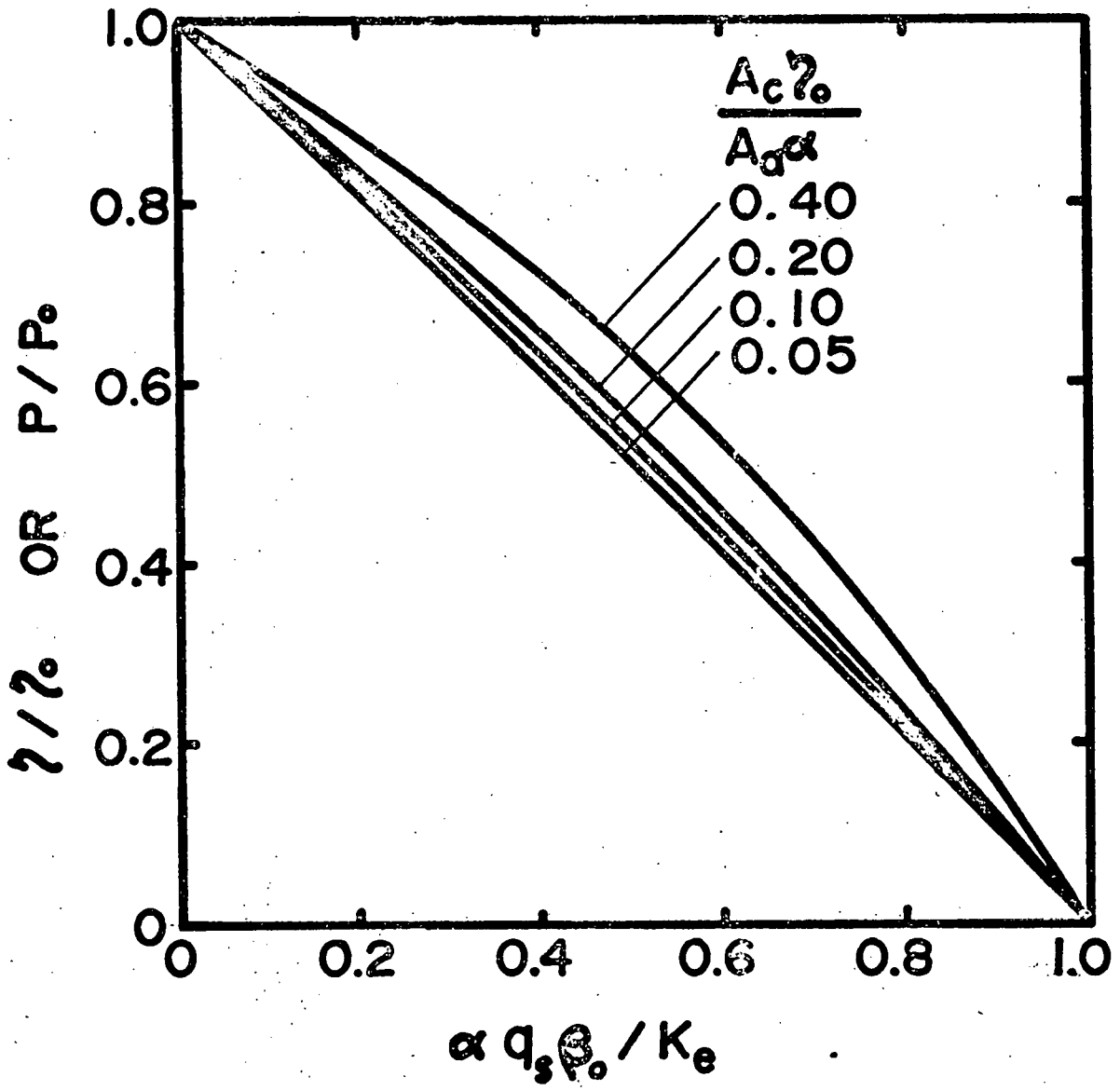

Fig. 1 Normalized power output vs. normalized solar irradiation.

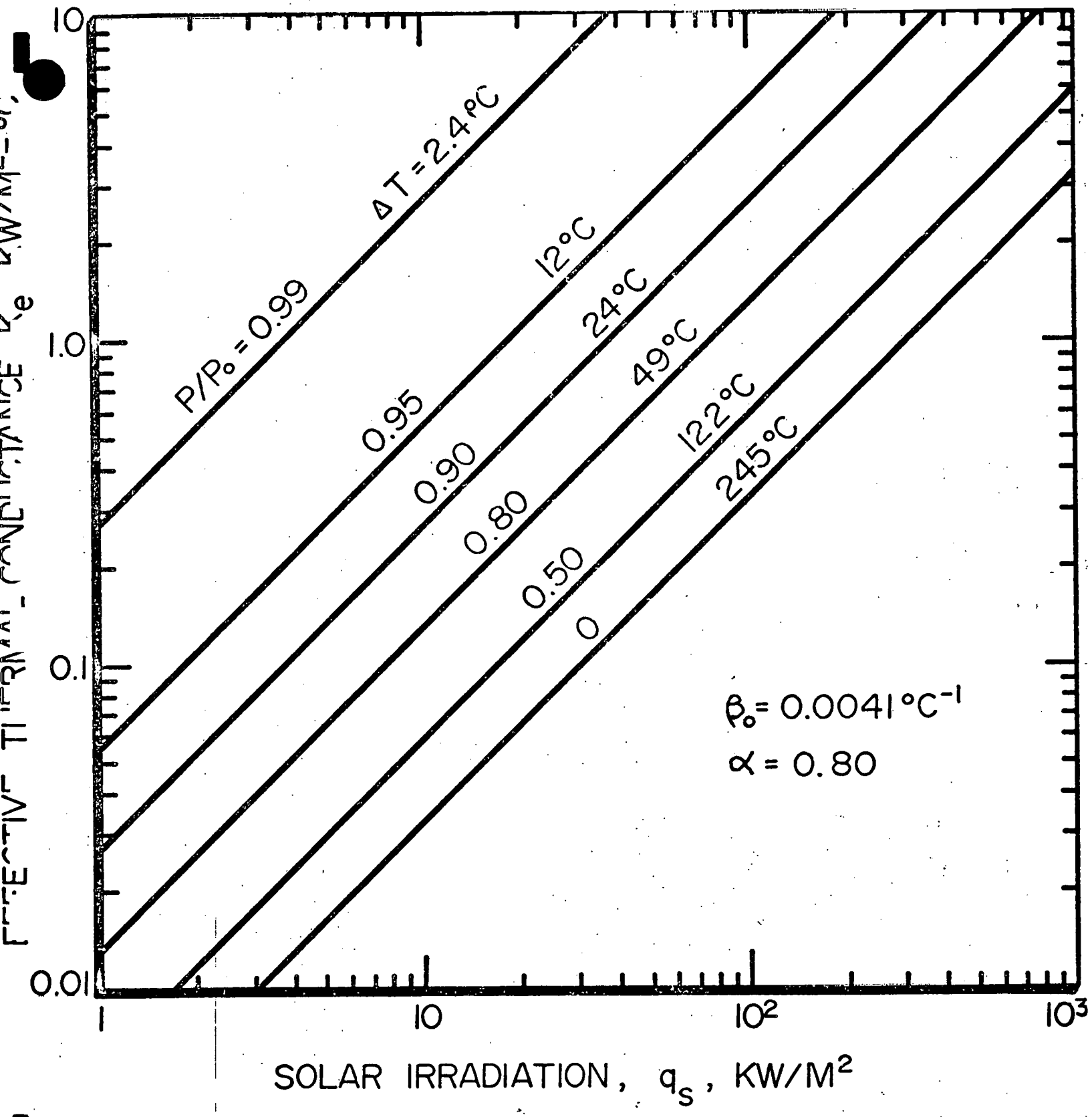

Fig. 2 Effective thermal conductance requirement vs. solar irradiation for silicon cells with output at various fractions of that for limiting case of cells operating at coolant temperature. Temperature rise of cell above coolant (T_o = 25°C) is also indicated.

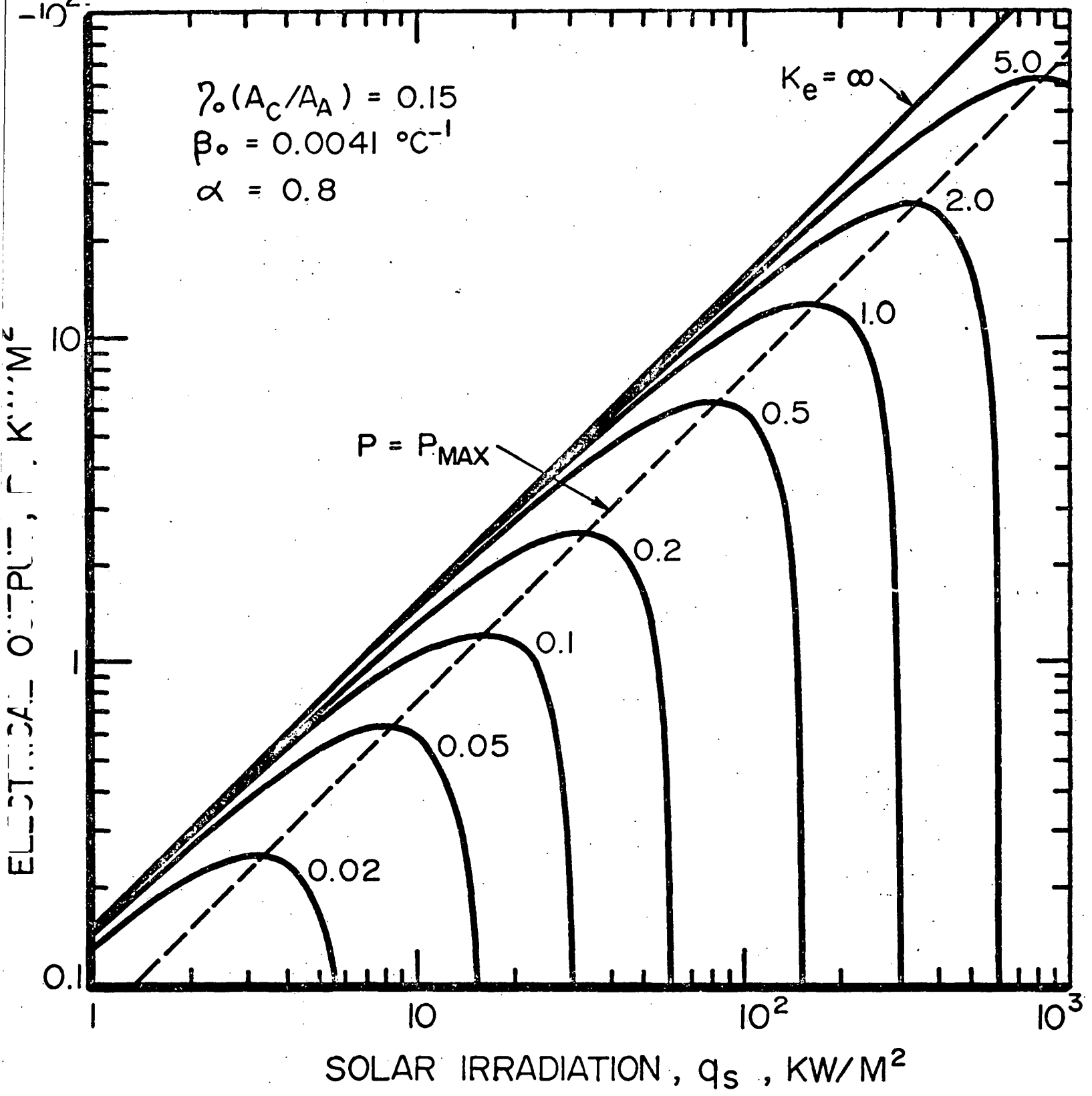

Fig. 3 Electrical output of silicon cells vs. solar irradiation for various effective thermal conductances.

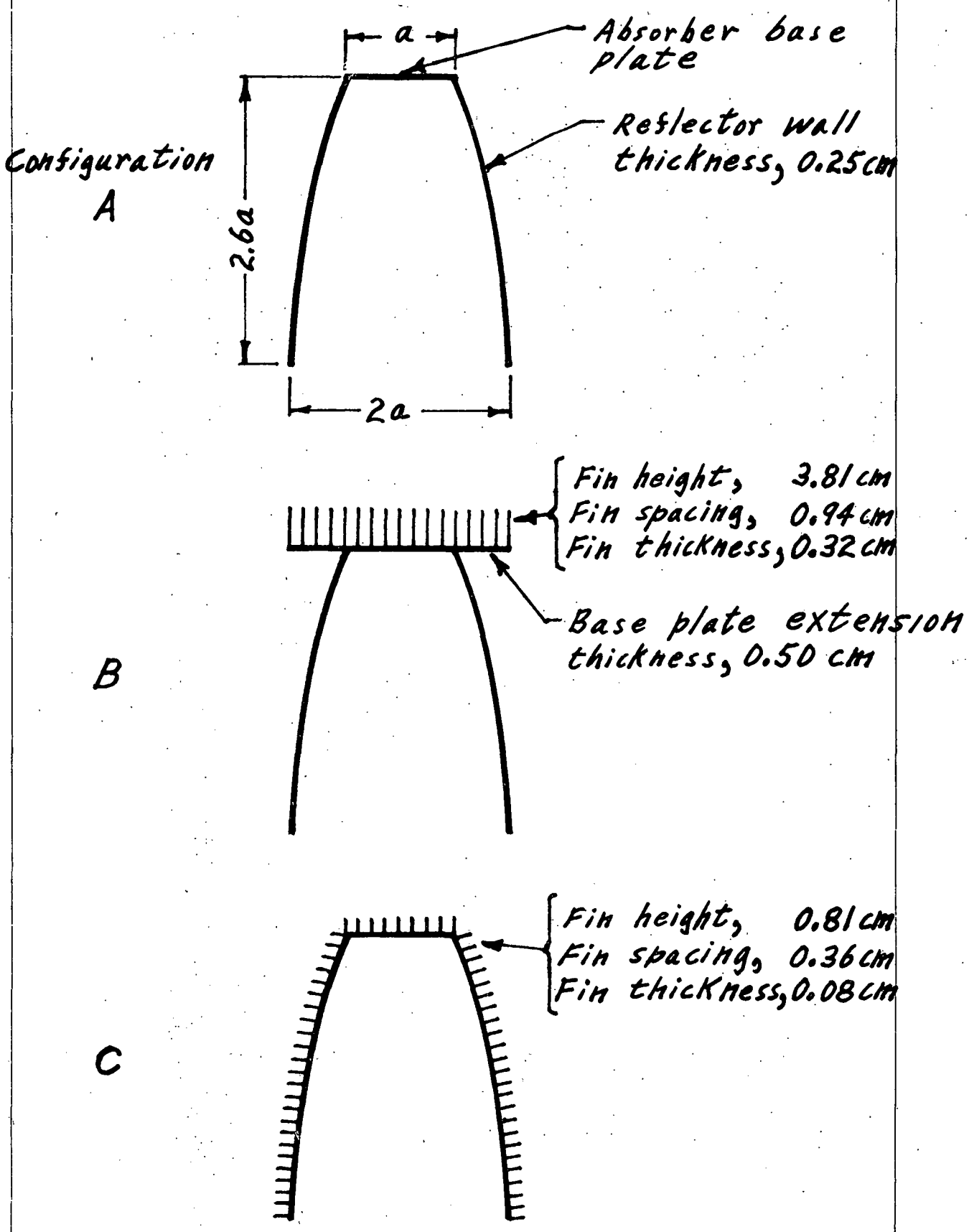

Fig. 4 Examples of alternative configurations for passive cooling.

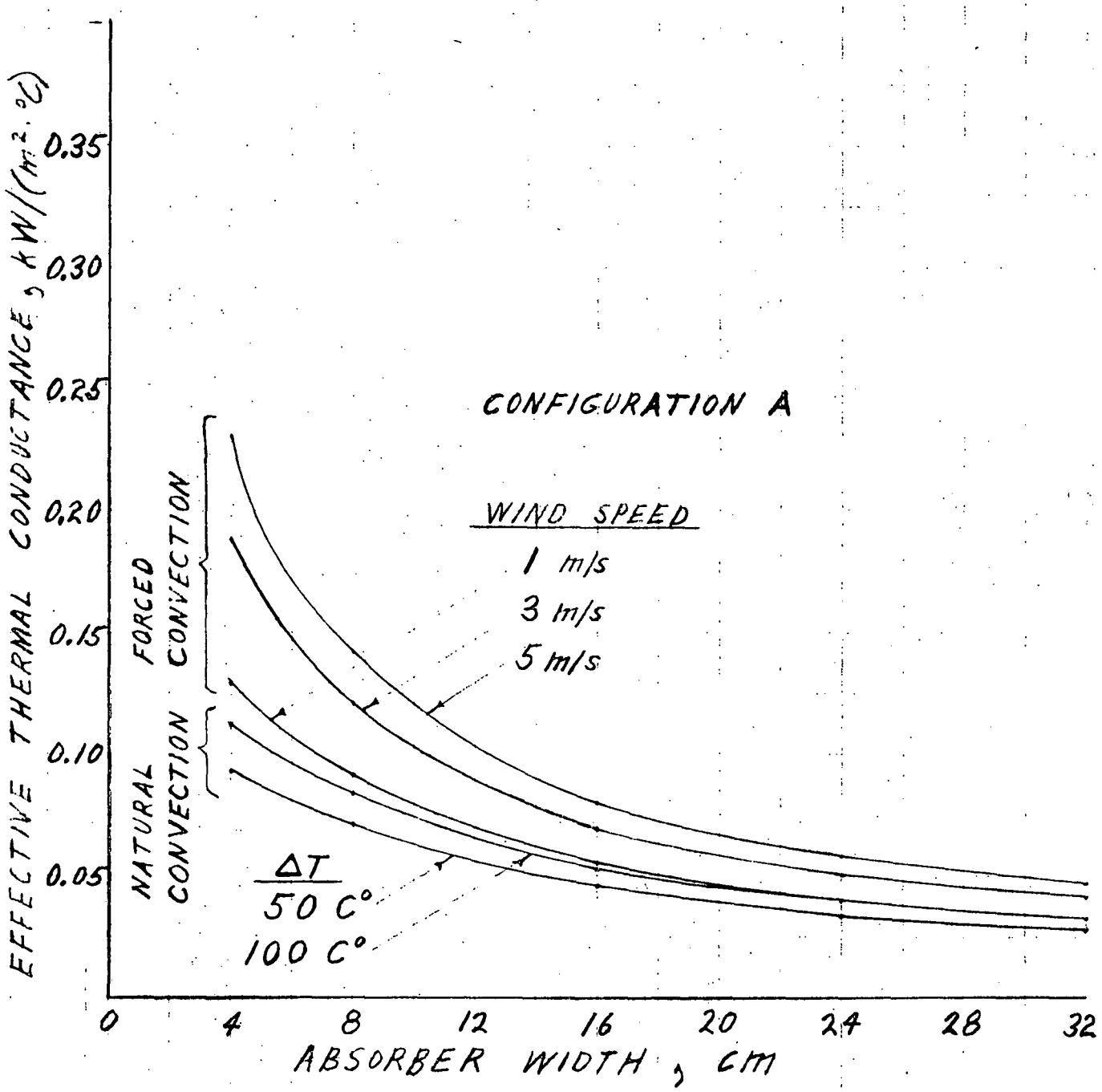

Fig. 5 Estimated effective thermal conductance values for basic CPC configuration.

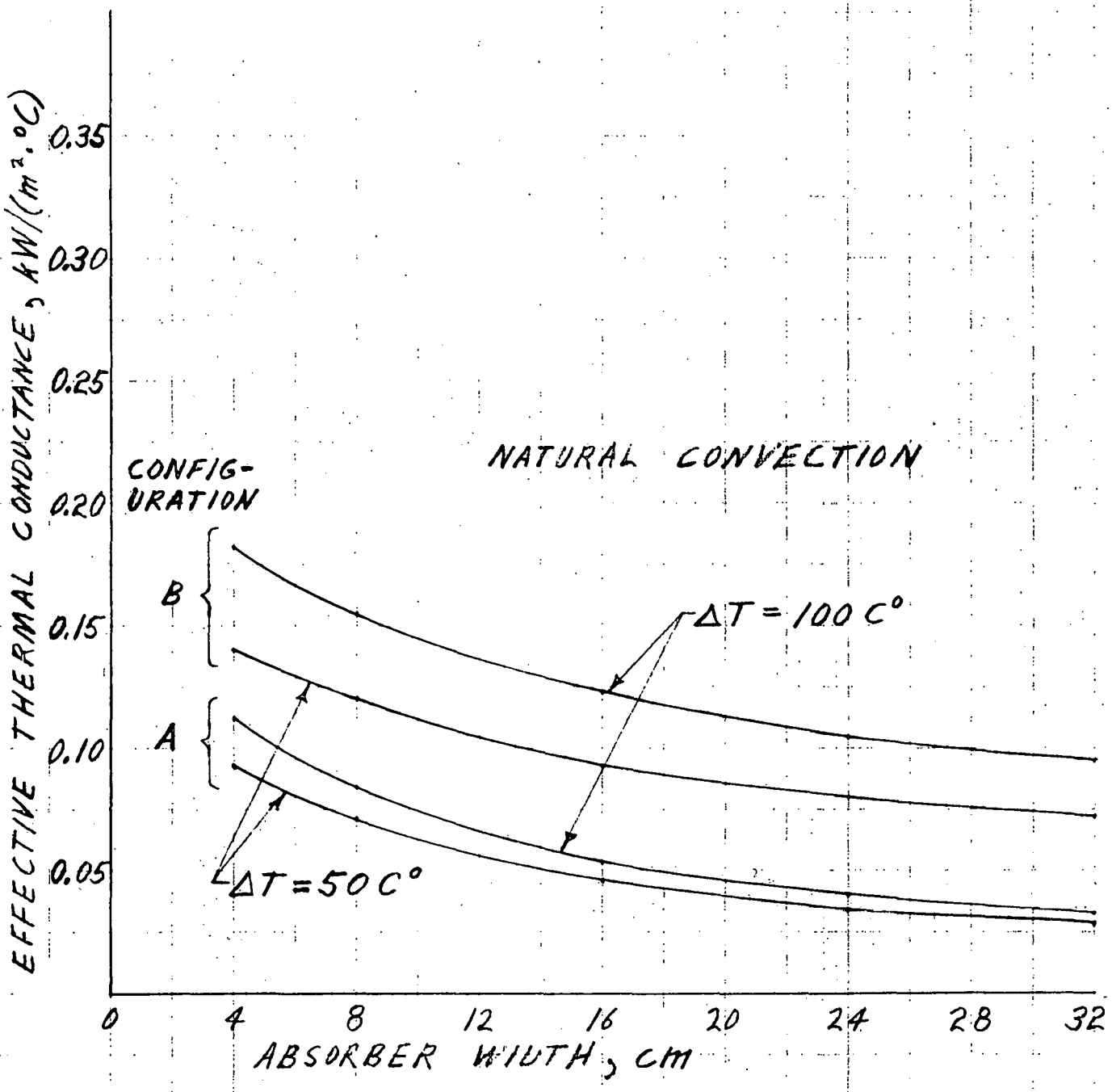

Fig. 6 Illustration of effect of adding straight fins to basic CPC configuration for case of natural convection.

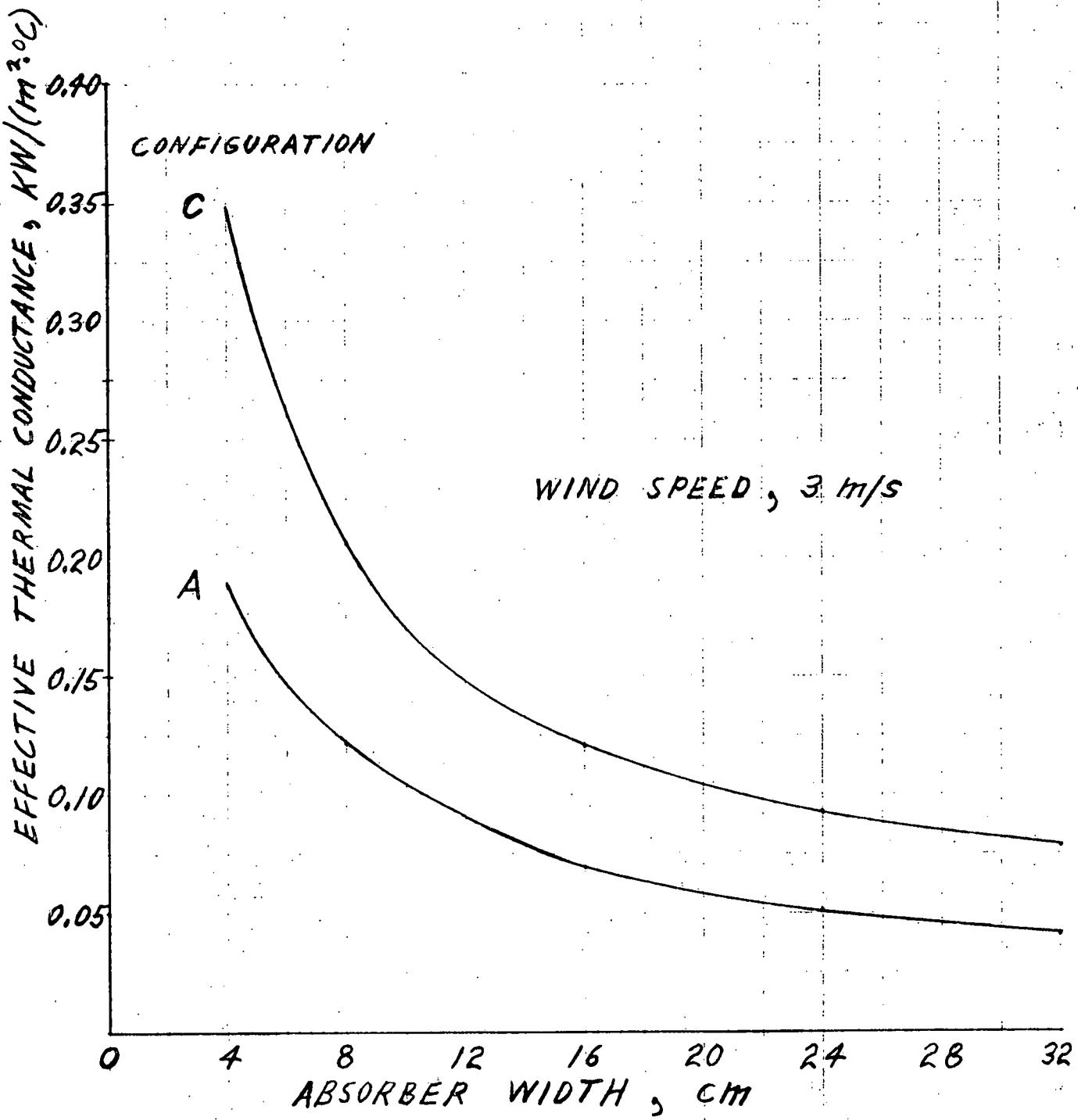

Fig.7 Illustration of effect of adding straight fins to basic CPC configuration in presence of wind.

Fig. 8 Parameters for example cases of water cooling.

Case*	Flow Velocity (m/s)	Flow Rate** (Kgm/s)	Configuration	K ($kW/m^2 \cdot °C$)	Ke ($kW/m^2 \cdot °C$)
A	0.6	0.16	I	2.2	1.2
B			II	1.4	0.54
C	3.0	0.79	I	3.1	2.5
D			II	1.8	1.2

*All cases: Flow channel length, 12.2 m
Cell/Heat-sink bond thermal conductance, 4 $kW/m^2 \cdot °C$
Flow channel wall thickness, 0.15 cm

** per flow channel

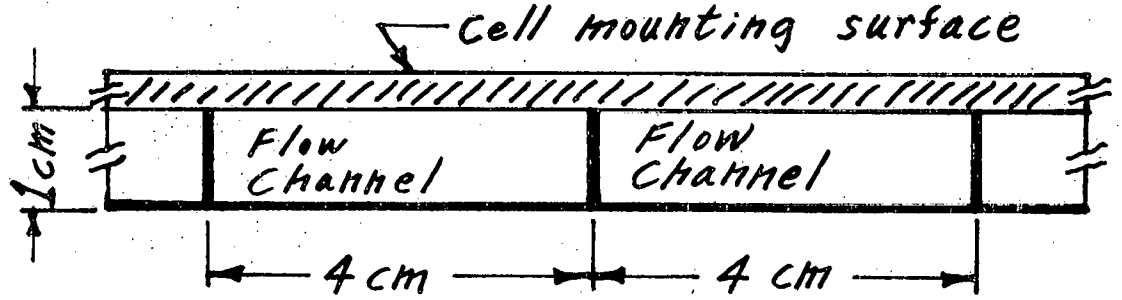

Configuration I

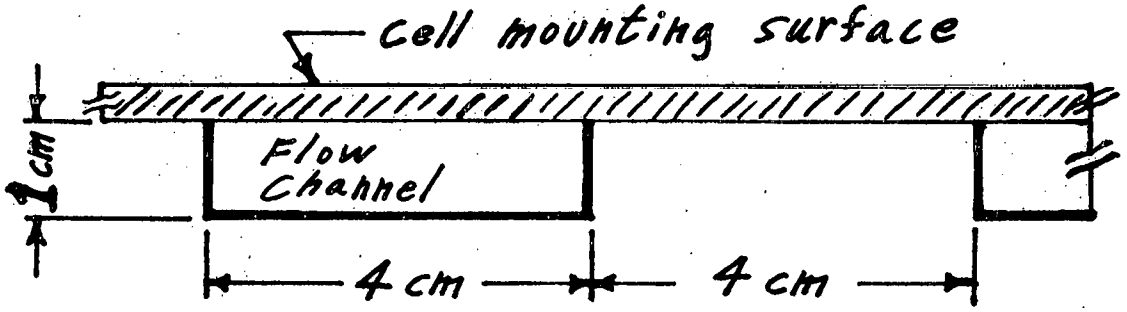

Configuration II

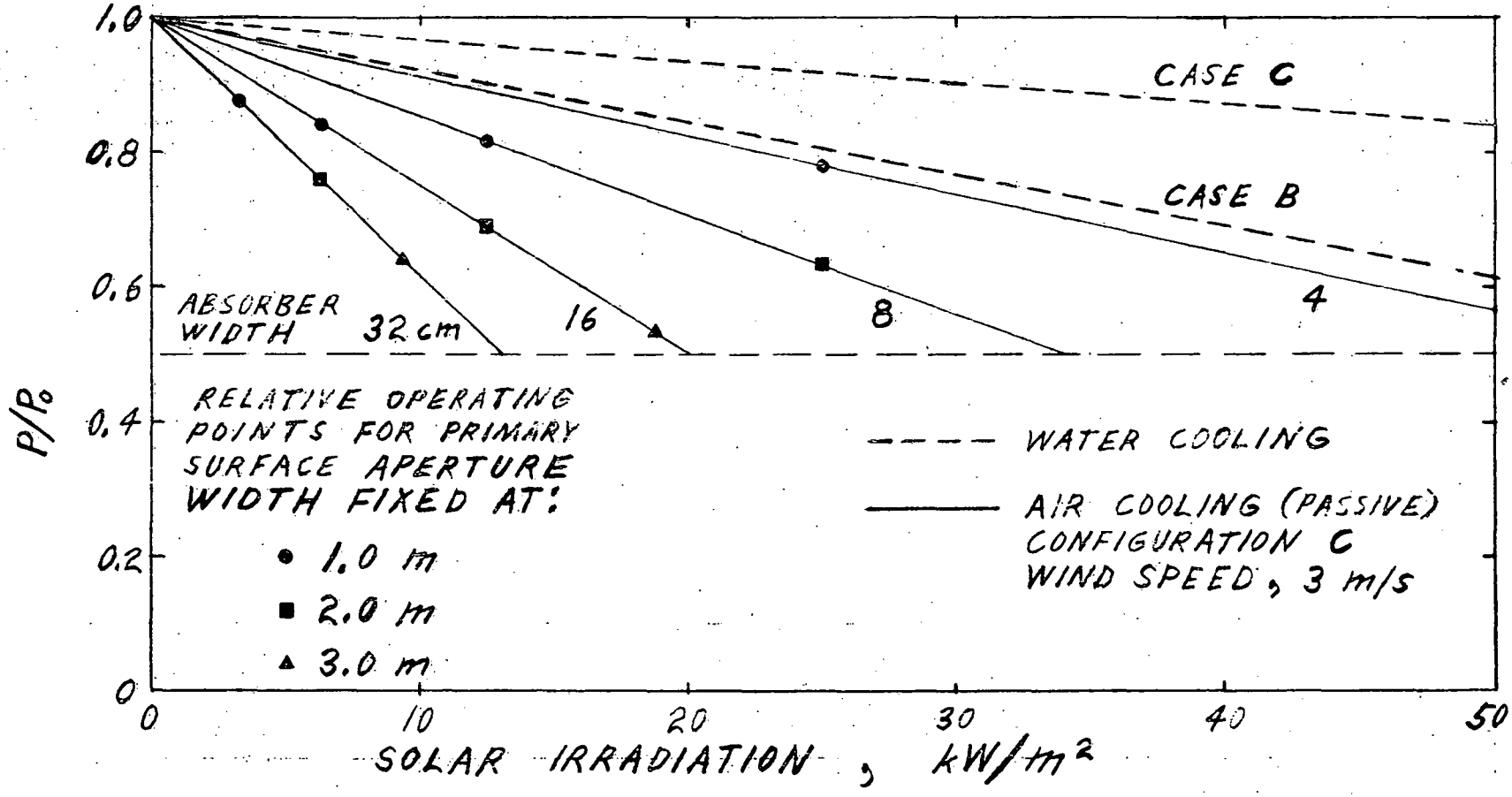

Fig. 9 Estimated cell output relative to that for cells at ambient temperature as a function of solar irradiation on cells for several cooling conditions.

COST-EFFECTIVENESS CALCULATIONS

The 1974 annual report to the National Science Foundation under NSF Grant GI-41894, "Terrestrial Photovoltaic Power Systems with Sunlight Concentration" by Arizona State University and Spectrolab, contained cost-effectiveness calculations relevant to this program. No new calculations were made under this program, because the time and information available was insufficient to allow us to improve substantially on the earlier calculations. This chapter therefore is an interpretation of the earlier calculations in the light of the results presented in previous chapters.

In the NSF report, the cost model used was an extremely simple one which nevertheless provides insight into the effects of changing parameters on electricity costs. Only the fixed charge component of electricity cost was computed; operating and maintenance costs were not included. It was assumed that all electricity generated could be utilized. Actual insolation data for Albuquerque 1962, from Aerospace Corporation tapes, was utilized to determine annual output. A fixed charge ratio of 18% was assumed, which is reasonable for a privately-owned utility. Concentration ratios were calculated assuming a concentrator optical transmission factor of 0.85 and a ratio of cell area to absorber area of 0.85. Cell series resistance losses were <u>not</u> included in the calculations, since it had been shown earlier that such losses can always be made negligible by proper cell design (of course, with some penalty in cell cost or unconcentrated efficiency or both).

Figures 7.6 through 7.11 are taken from the NSF report and show the results of these calculations. X is absorber cost, Z is land cost, and Y includes all other capital costs (mainly the concentrator and tracking system). Values for Y were taken from various NSF and NASA reports dealing with solar-thermal collector designs, and the values sued in the calculations were $\$15/m^2$ for flat unconcentrated arrays, $\$45/m^2$ for linear focus concentrators with single-axis tracking, and $\$60/m^2$ for systems with two-axis tracking. For comparison, Table 7.6 gives energy cost for fixed unconcentrated arrays, calculated on a similar basis.

It is evident that the addition of an optical concentrator to a photovoltaic system will be advantageous only if the cost per unit aperture area of the concentrator is substantially less than the cost per unit area of photovoltaic cells, since the use of a concentrator reduces the total amount of sunlight available for conversion because of loss of diffuse sunlight and optical losses in the concentrator. This effect can be seen by comparing the curves in Figures 7.7 and 7.10 for X = $\$50/m^2$ with the energy cost ($.034/kwh) from Table 7.6 for a fixed unconcentrated array with X = $\$50/m^2$, 15% cell efficiency. Values of Y less than $\$40/m^2$ are required for any improvement in energy cost.

If the ratio X/Y is large, a large saving can be obtained by concentration. The concentration ratio for minimum energy cost depends primarily on the effect of temperature on cell efficiency. Figures 7.6, 7.8, 7.9 and 7.11 show the effect of improving heat transfer efficiency

(increasing K_e). For these calculations, the only efficiency term included which varied with concentration ratio was the cell efficiency/temperature coefficient. If enough information had been available to permit estimating other efficiency coefficients (e.g., variation in concentrator transmission coefficient with concentration ratio) similar effects would be seen; i.e., the minimum cost would occur at the point at which the loss of system conversion efficiency with increasing concentration just balances the cost saving from reduction in cell area. For any particular concentrator design, optical efficiency might vary somewhat with concentration ratio but one would not expect much variation if the best configuration were chosen at each value of concentration. Therefore the inclusion of more efficiency terms would not be expected to produce a substantial change in the plotted curves.

In summary, the important characteristics of a concentrator for use with photovoltaic cells are the cost of the concentrator per unit of aperture and the uniformity of illumination produced at the absorber. The cost savings obtainable through concentration depend on reducing the system cost per unit aperture area by replacing expensive cells with less expensive optics while maintaing system efficiency as high as possible. The only important way in which the concentrator design strongly affects system efficiency is through uniformity of illumination, which strongly affects cell efficiency.

The two-element concentrator analyzed in the preceding chapters of this report appears to be superior to any single-element concentrator

because it should be little more expensive than the least expensive single-element concentrator, while it is far superior in uniformity. The cost of the two-element concentrator is nearly entirely contained in the cost of the primary element. For example, for the design for δ - 2.5° analyzed in chapters 3 and 4, the additional cost of the secondary element fabricated as an aluminum extrusion is estimated at less than $2 per square meter of primary aperture, and from this a credit for the cell support and heat sink which it replaces should be subtracted, reducing the net cost to nearly zero.

The optimum concentration ratio for the complete system depends on the ratio of cell to concentrator cost, the type and accuracy of tracking, the effective heat transfer coefficient, and other factors. Generally it can be expected to lie in the range of 5 to 100. As discussed in Chapter 2, this range can be covered by at most two CEC designs, which is another advantage of the two-element concentrator.

CONCLUSIONS

Despite the short time available for this program and the resulting lack of completeness of this report, we believe that enough has been done to justify the conclusion that the two-element concentrator is superior to any single-element concentrator for use in photovoltaic systems. The main purpose of this Chapter of the report is to present some recommendations on further work to complete the analysis of this concentrator and to develop specific designs for specific applications.

In Chapter 2, a number of possible choices for the primary element were briefly discussed. It would be desirable to evaluate each of these, and possibly others, in more detail by ray tracing in the manner of the analysis in Chapter 3. Since low cost of the primary element is a major consideration, the effects of errors in surface figure of the primary element should also be considered to determine the tolerances with which this element must be fabricated. The ray tracing program developed by us has this capability.

More detailed cost-effectiveness calculations are desirable but merely adding more parameters to the calculation does not seem attractive to us. A more useful approach would be to choose some specific applications, define them in a clear and detailed manner, and then work up detailed designs for cost comparisons.

In this connection, we think that further calculations for systems involving horizontal EW troughs with periodic tilt adjustment should be made. Existing calculations (e.g., ANL Report SOL 75-02) are based on a

requirement of a minimum number of hours of collection. It is not intuitively obvious to us that this requirement leads to a near-optimum interval between adjustments. It would be interesting to determine the acceptance half angle for lowest energy cost, for a specified number of adjustments per year. In the NSF report there are some calculations on the CPC concentrator which can be further manipulated to give the optimum acceptance half angle. For daily adjustment (the only case calculated) the optimum is 2° to 3°, which leads to a concentration ratio of the order of 20. This is much more than we anticipated before performing the calculations.

In any case, the evaluation of different possibilities for orientation adjustment or tracking clearly should be done in the context of a specific application. This is also true of structural requirements and estimation of manufacturing costs.

The final step would be to build prototypes of one or more of the specific designs and experimentally determine their performance. It would be desirable to arrive at this point as quickly as possible, and we believe that both the additional analysis and the prototype fabrication could be done within a 12 to 18 month program.